TAMPEREEN TEKNILLINEN YLIOPISTO
TAMPERE UNIVERSITY OF TECHNOLOGY

Mari Honkanen

Injection-Molded Hybrids – Characterization of Metal-Plastic Interfacial Features

Julkaisu 993 • Publication 993

Tampere 2011

Tampereen teknillinen yliopisto. Julkaisu 993
Tampere University of Technology. Publication 993

Mari Honkanen

Injection-Molded Hybrids – Characterization of Metal-Plastic Interfacial Features

Thesis for the degree of Doctor of Science in Technology to be presented with due permission for public examination and criticism in Konetalo Building, Auditorium K1702, at Tampere University of Technology, on the 11th of November 2011, at 12 noon.

Tampereen teknillinen yliopisto - Tampere University of Technology
Tampere 2011

ISBN 978-952-15-2665-7 (printed)
ISBN 978-952-15-2673-2 (PDF)
ISSN 1459-2045

ABSTRACT

Injection-molded metal-plastic hybrids are innovative products combining dissimilar materials and their properties in the same component. The hybrids can offer benefits which are not achieved with individual material alone e.g.: savings in weight, part reduction, better dimensional stability, and manufacturing multi-functional components in a few processing steps. However, joining of physically and chemically different materials is very challenging. Bonds between metals and plastics can be achieved by chemical or physical bonding mechanisms or by mechanical interlocking like perforating a metal insert and over-molding polymer on it, which is the mainly used method in the industrial applications. In many applications like in electronic components, planar inserts without perforation are needed, but a detailed knowledge of the chemical adhesion between metal and plastic is still lacking.

In this study, metal-plastic hybrid structures were produced by injection molding and the chemical adhesion between metal and plastic was achieved with coupling agent. Stainless steel, AISI 304, and coppers, OFE-OK and Cu-DHP, were used as metallic inserts and thermoplastic urethane (TPU) was used as a plastic component and aminofunctional silane was used as coupling agent. The bonding of silane to as-received metal surfaces was poor, so active surface pre-treatments, i.e. electrolytical polishing and oxidation treatments, for metals were needed to improve the bonding. Manufacturing of the metal-plastic hybrids consisted of three steps: (1) surface modification of metal, (2) silane treatment of modified metal, and (3) injection molding of plastic onto silane-treated metal. The hybrid structures were characterized within each manufacturing step. Prior to silane treatment, metal surfaces were characterized with atomic force microscopy (AFM), transmission electron microscopy (TEM), reflection absorption infrared spectroscopy (RAIRS), and X-ray photoelectron spectroscopy (XPS). Scanning electron microscopy (SEM), AFM, TEM, RAIRS, and XPS were used to study the silane layers. The finished hybrid parts were characterized with SEM and the adhesion strengths of the hybrids were measured with peel tests. AFM, SEM, and RAIRS were used to find out the failure types of the hybrids in peel.

According to comprehensive characterization results, a controlled oxide layer on the metal surface was needed to achieve a uniform and cross-linked silane layer with amino species on the surface to react with plastic; a smooth metal surface produced by electrolytical polishing with a native oxide layer was not enough. The hybrids manufactured with the oxidized metal inserts failed mainly cohesively in the plastic part with high peel strength values while the hybrids manufactured with the as-received or electrolytically polished inserts failed mainly inside the silane layer with poor peel strength values due to uneven formation of the silane layers. So the metal surface, prior to silane treatment, had a significant effect on the silane layer formation and hence the adhesion strength values of the related hybrids; similar strength values were achieved with similar pre-treatments of the metal surfaces regardless of metal used.

PREFACE

This work was carried out in Department of Materials Science (DMS) at Tampere University of Technology (TUT). First and foremost, I want to thank my supervisors Prof. Toivo Lepistö and Dr. Minnamari Vippola for the opportunity to work under their excellent guidance and for their continuous encouragement and support during the years and for their valuable discussions and comments on my work.

I express thanks to M.Sc. Maija Hoikkanen and Prof. Jyrki Vuorinen from Laboratory of Plastics and Elastomer Technology in DMS for their valuable co-operation and fruitful discussions during the studies of the hybrid structures. In addition, I want to thank all of my colleagues, past and present, in DMS and especially in Laboratory of Materials Characterization for enjoyable working atmosphere. Special thanks are due to the research assistants who have helped me in this work. Acknowledgement is also due to Prof. Mika Valden and his group, Surface Science Laboratory at TUT, for XPS measurements.

Graduate School of Processing of Polymers and Polymer-based Multimaterials (POPROK), Finnish Funding Agency for Technology and Innovation (TEKES), Finnish industry, Jenny and Antti Wihuri Foundation, Kaupallisten ja teknillisten tieteiden tukisäätiö (KAUTE), and City of Tampere are acknowledged for financial support.

I want to thank all my friends for inspirational free time. In addition, I am very grateful to my whole family, especially to my parents Tarja and Timo and my sister Kaisa and her husband Vesa for their endless care, support, and understanding over the years. Then, my special thanks go to Jere, Jenna, and Melissa for the arrangement of funny leisure-time activities for me – with you, I was really able to detach from my hard work. Finally, the deepest thanks go to my dear Kai for his love, care, endless encouragement, and incredible patience during the years.

Kangasala, October 2011

Mari Honkanen

TABLE OF CONTENTS:

LIST OF ORIGINAL PUBLICATIONS

This thesis is based on the original experimental work presented in detail in the following six publications. They are referred in the text with Publications I-VI.

I Mari Honkanen, Minnamari Vippola and Toivo Lepistö, Characterisation of Stainless Steel Surfaces – Modified in Air at 350°C, *Surface Engineering* 27 (2011) 325-331.

II Mari Honkanen, Maija Hoikkanen, Minnamari Vippola, Jyrki Vuorinen and Toivo Lepistö, Metal-Plastic Adhesion in Injection-Molded Hybrids, *Journal of Adhesion Science and Technology* 23 (2009) 1747-1761.

III Mari Honkanen, Maija Hoikkanen, Minnamari Vippola, Jyrki Vuorinen, Toivo Lepistö, Petri Jussila, Harri Ali-Löytty, Markus Lampimäki and Mika Valden, Characterization of Silane Layers on Modified Stainless Steel Surfaces and Related Stainless Steel-Plastic Hybrids, *Applied Surface Science* 257 (2011) 9335-9346.

IV Mari Honkanen, Minnamari Vippola and Toivo Lepistö, Low Temperature Oxidation of Copper Alloys – AEM and AFM Characterization, *Journal of Materials Science* 42 (2007) 4684-4691.

V Mari Honkanen, Minnamari Vippola and Toivo Lepistö, Oxidation of Copper Alloys Studied by Analytical Transmission Electron Microscopy Cross-Sectional Specimens, *Journal of Materials Research* 23 (2008) 1350-1357.

VI Mari Honkanen, Maija Hoikkanen, Minnamari Vippola, Jyrki Vuorinen and Toivo Lepistö, Aminofunctional Silane Layers for Improved Copper-Polymer Interface Adhesion, *Journal of Materials Science* 46 (2011) 6618-6626.

AUTHOR'S CONTRIBUTION

In the publications I, IV, and V, Mari Honkanen was the main researcher and author. She planned and organized experiments, performed TEM and AFM sample preparations and characterizations, and analyzed the results. Prof. Toivo Lepistö and Dr. Minnamari Vippola, the supervisors, gave advises on the experimental parts and commented the manuscripts.

In the publications II, III, and VI, Mari Honkanen was the main author and planned and organized experiments together with M.Sc. Maija Hoikkanen. Mari Honkanen carried out AFM, SEM, and TEM sample preparations and characterizations, and analyzed the results. Maija Hoikkanen participated manuscript writing and was responsible for the injection molding process, the peel tests, and the RAIRS studies (in the publication VI), and the analysis of these results. Dr. Minnamari Vippola, Prof. Toivo Lepistö, and Prof. Jyrki Vuorinen gave advises on the experimental parts and commented the manuscripts. Dr. Petri Jussila was together with M.Sc. Harri Ali-Löytty, Dr. Markus Lampimäki, and Prof. Mika Valden responsible for XPS studies, analysis, and reporting (in the publication III).

LIST OF SYMBOLS AND ABBREVIATIONS

a, b, and c	Lattice parameters
γ-AEAPS	N-(β-aminoethyl)-γ-aminopropyltrimethoxysilane
AISI	American iron and steel institute
AISI 304	Cr-Ni stainless steel
AISI 316L	Cr-Ni-Mo stainless steel
APS	Aminopropyltriethoxysilane
γ-APS	γ-Aminopropyltriethoxysilane
ASTM	American society for testing and materials
BCC	Body-centered cubic structure
BTSE	Bis-1,2-(triethoxysilyl)ethane
CH_2	Methylene
CH_3OH	Methanol
Cr_2O_3	Chromium oxide
CuAg	Oxygen-free silver-alloyed copper
Cu-DHP	Phosphorus deoxidized copper
CuO	Copper oxide
Cu_2O	Copper oxide
d	Lattice plane spacing value
EN	European standard
FCC	Face-centered cubic structure
FeO	Iron oxide
Fe_2O_3	Iron oxide
Fe_3O_4	Iron oxide
γ-GPS	γ-Glycidoxypropyltrimethoxysilane
H_2O	Water
Me	Metal
Me_xO_y	Metal oxide
Me_2O_3	Metal oxide
MeOH	Hydroxyl group on metal surface
MeOSi	Covalent oxane bond between metal and silicon
NH, NH_2	Amine
O_2	Dioxygen
OCH_3	Methoxy
OC_2H_2	Ethoxy
OF-OK	Oxygen free copper (O_2 max. 10 ppm)
OFE-OK	Oxygen free copper (O_2 max. 5 ppm)
OR	Hydrolysable alkoxy group
PVC	Polyvinyl chloride
ROH	Alcohol
SiOH	Silanol group
SiOSi	Siloxane
TPU	Thermoplastic urethane
X	Hydrolysable group
Y	Organofunctional group

AFM	Atomic force microscopy
AsB	Angular selective backscattered electron
EDS	Energy dispersive spectrometry
FESEM	Field-emission scanning electron microscopy
NMT	Nano-molding technology
PIPS	Precision ion polishing system
PMH	Plastic-Metal Hybrid
R_a	Arithmetical mean roughness of surface
RAIRS	Reflection-absorption infrared spectroscopy
SAED	Selected area electron diffraction
SE	Secondary electron
SEM	Scanning electron microscopy
TEM	Transmission electron microscopy
XPS	X-ray photoelectron spectroscopy

1. INTRODUCTION

"Hybrid" is the Greek word and means different origin and properties of materials [1]. Injection-molded metal-plastic hybrids are innovative products combining dissimilar materials and their properties in the same component in a few processing steps. The hybrids can offer benefits which are not achieved with individual material alone e.g.: savings in weight, part reduction, better dimensional stability, and manufacturing multi-functional components in a few processing steps. Metal-plastic hybrids can replace metal structures for example in cars, household appliances, and sporting goods [1–3].

Joining of metals and plastics together is, however, very challenging. This is because of the fact that two physically and chemically very different materials have to be combined. This difference causes poor adhesion between a metal insert and plastic component, shrinkage of plastic, residual stresses and hence bending of the hybrid structure [4]. Bonds between metals and plastics can be achieved by chemical or physical bonding mechanisms or by mechanical interlocking like perforating a metal insert and over-molding plastic on it, which is the mainly used method in the industrial applications [1,3,5]. However, in many applications, like in electronic components, planar inserts without perforation are needed, but a detailed knowledge of the chemical adhesion between metal and plastic is still lacking.

Coupling agents are chemicals which improve adhesion between two or more dissimilar constituents such as plastic and metal. Nowadays, silanes are the most commonly used coupling agents [6–8]. Silane used must be reactive with plastic, adhere well to the metal surface, and form a uniform thin layer on metal. Especially production of a uniform silane layer on the metal substrates can be challenging [9–13]. In addition, the substrate surface and silane treatment parameters have a significant effect on the silane layer structure and hence the metal-plastic adhesion [14,15].

The aim of this work was to produce well-bonded stainless steel-thermoplastic urethane and copper-thermoplastic urethane hybrid structures. Bonding between metals and plastic was produced by silane. The bonding of silane to the industrially finished metal surfaces was poor, so surface modifications, i.e. polishing and oxidation, for stainless steel and copper surfaces were needed to achieve thin, uniform, and cross-linked silane layers and hence well-bonded metal-plastic hybrids. The metal surface structures and silane layers on them were characterized with atomic force microscopy (AFM), scanning electron microscopy (SEM), transmission electron microscopy (TEM), reflection absorption infrared spectroscopy (RAIRS), and X-ray photoelectron spectroscopy (XPS). The adhesion strength values of the metal-plastic hybrids were measured with peel-tests and peeled fracture surfaces were studied with AFM, SEM, and RAIRS.

In addition to this introduction, this thesis consists of five chapters. Chapter 2 contains an introduction to metal-plastic hybrids; their manufacturing and related phenomena like joining of metal and plastic, metal surface pre-treatments, and oxide structures on the metal surfaces. Chapter 3 describes the aim of the present study. Chapter 4, the experimental part, presents materials and the manufacturing steps of the hybrid structures and introduces briefly the characterization methods. Chapter 5, the result and discussion part, focuses on the main results concerning the stainless steel-plastic and copper-plastic hybrids; the metal oxide structures and their effect on the formed silane layers and hence on the adhesion strength and failure types of the metal-plastic hybrids. Chapter 6 consists of concluding remarks. In addition, six original publications are in the appendix.

2. METAL-PLASTIC HYBRIDS

Metal-plastic hybrids combine dissimilar materials and their different properties in the same component. In the metal-plastic hybrids, engineering plastics are used to e.g. improve wear resistant and to reduce weight and metals are used to e.g. improve strength and conductivity [16]. In the industrial applications, metals used are mainly aluminum and stainless steel and plastics are e.g. polyamide, polybutylene, and elastomers [1,4,17]. Traditionally, for example in the automotive industry, metals and plastics have been competing materials but nowadays, those two different materials are combined to one component and they are replacing metallic structures [18].

In the 1980s, the patented Plastic-Metal Hybrid (PMH) design technology was introduced by Bayer. Later in 2004, the patent was transferred to Lanxess Corporation. Audi was the first automotive manufacturer who used PMH technology in practice. At the end of 1996, it produced the front end of the Audi A6 as a hybrid structure combining a metal profile and a elastomer-modified polyamide part together; the metal profile was placed in the mold and plastic was injection-molded on the profile. The adhesion was achieved by wrapping plastic over the metal part or by mechanical interlocking through the holes of the metal profile. Nowadays, e.g. Audi, Ford, and Nissan are using PMH technology in the front end and door structures, seating, etc. resulting for example 10 % reduction in the manufacturing costs and 15 % reduction in weight [1,3,5]. In addition of automotive industry, metal-plastic hybrids are used for example in appliances, laptops, and sporting goods [2]; some applications are presented in Fig. 1 [1,16,17].

Figure 1. *Metal-plastic hybrid applications in automotive and electronic industry and in sporting goods and household appliances by Lanxess, Taiseiplas, and InserTech, modified from [1,16,17].*

2.1. Manufacturing of metal-plastic hybrids

In the industrial applications, the main manufacturing technique used for the metal-plastic hybrids is the injection molding process; a metal sheet is inserted in the mold and plastic is injected onto the sheet. Adhesion between materials is mainly based on the mechanical interlocking by perforating the metal insert and by overmolding plastic on it. The steps of the manufacturing process of the door structure by Lanxess are presented in Fig. 2; opened mold, perforated metal insert in the mold, and finished injection-molded metal-plastic hybrid [1]. In addition of Lanxess, for example companies InserTech and Taiseiplas are manufacturing injection-molded metal-plastic hybrids. InserTech has produced wide range of metal-plastic hybrid structures with insert injection molding process, like: cellular phone antenna, speaker connectors, baskets, and frames, automotive connectors, and electro-surgery blades. InserTech uses insert injection molding with three different variations: single encapsulation, pre-mold/overmold, and two shot molding. With pre-mold/overmold technique complicated parts can be manufactured because injection molding is carried out twice. In the two shot molding, two different colors or two different polymers are used. In the case of the single encapsulation, one shot of plastic encapsulates the metallic insert [19]. Taiseiplas uses elastomer + metal integration technology e.g. in cellular phones and liquid crystal screens. In that technique, a metal part is coated, cured, and inserted in the mold for further injection molding of elastomer on the metal part. Taiseiplas has also nano-molding technology (NMT) which integrates aluminum and plastic; an aluminum sheet is dipped in the solution and then resin is injection-molded on the sheet [17].

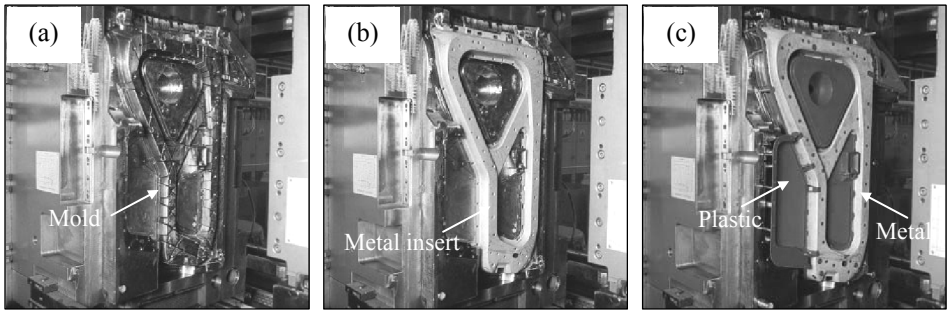

Figure 2. *Manufacturing process of metal-plastic hybrid in automotive industry, (a) open mold, (b) perforated metal insert in mold, and (c) finished injection-molded metal-plastic hybrid, modified from [1].*

2.2. Joining of metal and plastic with silane

Joining of two chemically and physically very dissimilar materials in the metal-plastic hybrids is challenging. Difference causes poor adhesion between metal insert and plastic component, shrinkage of plastic, residual stresses and hence bending of the hybrid [4]. Direct adhesion between them can be mainly produced by mechanical interlocking, modifying plastic chemically, or using coupling agents [3]. The mechanical interlocking is the mainly used method in industry but in many applications like in electronic components, planar metal inserts without perforation and hence chemical joining of metal and plastic is needed. However, no direct chemical bonds between metal and plastic are achieved due to the differences in their structure and surface reactivity [20]. So, to bond metal and plastic chemically together, coupling agents are required.

Coupling agents are chemicals which improve adhesion between two or more distinct constituents such as plastic and metal. Silanes are the most commonly used coupling agents to bond organic materials with inorganic materials. In the 1940s, silanes were started to use between glass fibers and organic resins. Nowadays, they have almost supplanted other coupling agents such as titanates, zirkonates, and chromium complexes. Titanate and zirkonate coupling agents were developed mainly for fillers. They can form bonds e.g. with calcium carbonate and boron which are not reactive with organosilanes. Chromium complexes improve adhesion between fibers and resin but nowadays because of their toxicity, they are mainly replaced by silanes [6–8,12].

2.2.1. Silane structure

Organosilanes are divided into three groups: functional, non-functional, and bifunctional organosilanes. The widely used functional organosilanes have typically a structure:

$$X_3Si(CH_2)_nY \quad (1)$$

where X is a hydrolyzable group (e.g. methoxy, ethoxy, or acetoxy) and Y is an organofunctional group (e.g. amino, methacryloxy, or epoxy) [7,21,22]. Non-functional silanes have typically a structure:

$$X_3Si(CH_2)_mSiX_3 \quad (2)$$

without organofunctional groups but with two SiX_3 groups at the ends. Bifunctional organosilanes have typically a structure:

$$X_3Si(CH_2)_nY_m(CH_2)_nSiX_3 \quad (3)$$

where Y, at the center, is e.g. an amine group or the chain of the sulfur atoms and SiX_3 groups are at the ends of the carbon chains. Nonfunctional and bifunctional silanes can be used for e.g. protection of the metal surfaces and as cross-linkers for silane coupling agents [21,22].

The best choice for metal-plastic hybrid applications is functional silane because it can bond to both metal, with hydrolysable group, and to plastic, with organofunctional group. Commercial functional silanes are usually alkoxy-based and the value of n is typically 3 so, they have a structure:

$$Y(CH_2)_3Si(OR)_3 \quad (4)$$

where OR is hydrolysable alkoxy group, for example methoxy (OCH_3) or ethoxy (OC_2H_5). Silicon at the center bonds to the organofunctional group and to the functional alkoxy group [21–24]. Some commercial coupling agents and their functional groups and suitability with plastics are presented in Table 1 [8]. Silane used should be chosen so that functional groups are reactive with plastic used [6].

Table 1. *Typical commercial coupling agents, their functional groups with polymer and substrate, and suitability with polymers [8].*

Chemical description (Abbreviation)	Functional group		Application (suitable polymers)
	With polymer	With substrate	
3-Chloropropyltrimethoxysilane	Chloro	Methoxy	Urethanes, Epoxy, Nylon, Phenolics, Polyolefins
Vinyltriethoxysilane (VES)	Vinyl	Ethoxy	Graft to Polyethylene for moisture crosslinking, EPDM, SBR, Polyolefin
γ-Methylacryloxypropyltrimethoxy-silane	Methacryloxy	Methoxy	Unsaturated Polyesters, Acrylics, EVA, Polyolefin
γ-Glycidoxypropyltrimethoxy-silane (GPMS)	Aliphatic epoxy	Methoxy	Epoxy, Urethanes, Acrylics, Polysulfides
γ-Mercaptopropyltrimethoxy-silane	Mercapto	Methoxy	Urethane, most organic rubber
γ-Aminopropyltriethoxysilane	Amino	Ethoxy	Acrylic, Nylon, Epoxy, Phenolics, PVC, Urethanes, Nitrile Rubber, Melamine
N-β-Aminoethyl-aminopropyl-trimethoxysilane (AAMS)	Amino	Methoxy	Acrylic, Nylon, Epoxy, Phenolics, PVC, Urethanes, Nitrile Rubber, Melamine

2.2.2. Silane bonding to metallic substrate

Silane has to be hydrolyzed to get it active to react with the substrate. Hydrolysis happens stepwise: hydrolysable alkoxy groups (OR) react with added water forming silanol groups (SiOH) and alcohol [8,21–25]:

$$YSi(OR)_3 + 3H_2O \leftrightarrow YSi(OH)_3 + 3ROH \quad (5)$$

Further, the reactive silanols start to condense to oligomers [8,25–27]:

$$YSi(OH)_3 + YSi(OH)_3 \leftrightarrow YSi(OH)_2OSi(OH)_2Y + H_2O \quad (6)$$

Based on the equations (5) and (6), the schematic drawing of the hydrolysis and condensation reactions of alkoxysilane with methoxy (OCH_3) as a hydrolysable alkoxy group (OR) is presented in Fig. 3. Hydrolysis is the fast process, within minutes, but condensation is much slower, within hours [7,26]. The functional groups and silane solution pH affect the rate of hydrolysis. The increasing order of the reactivity of the functional groups is propoxy, ethoxy, and methoxy. Hydrolysis is fast with low pH, it is very slow at neutral pH, and it is again very fast when pH is over 8 [23]. In addition, with low pH, the condensation rate of the SiOH groups is slower [28].

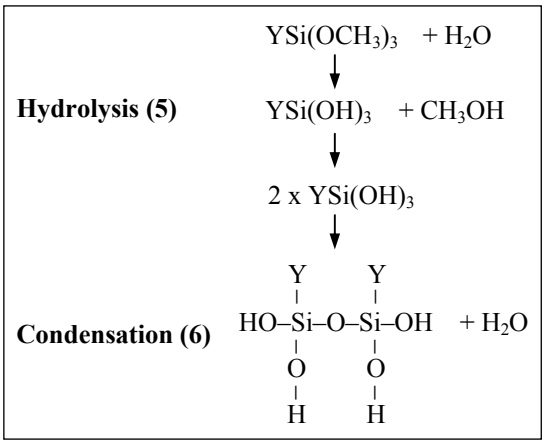

Figure 3. *Schematic drawing of hydrolysis and condensation reactions of alkoxysilane with methoxy (OCH_3) as hydrolysable alkoxy group (OR), based on equations (5) and (6).*

The condensation of silanol groups should be slight enough so that after hydrolysis, there are sufficient amount of active silanol groups to react with the substrate. When a substrate is immersed into the hydrolyzed silane solution, silanol groups react with hydroxyl groups (MeOH) on the metal surface [8,21,22,24], presented in the left side of the Fig. 4 (a) [24]. It is the fact that at the ambient condition, a hydrated layer always exits on the metal surface to react with silanol groups [14]. During drying and curing processes of the silane layers, two condensation reactions, (7) and (8), occur in the silane/metal interface: SiOH and MeOH form a stable and covalent oxane bond (MeOSi):

$$MeOH_{(metal\ surface)} + SiOH_{(solution)} \leftrightarrow MeOSi_{(interface)} + H_2O \quad (7)$$

and SiOH groups react with each other forming a siloxane network structure (SiOSi):

$$SiOH + SiOH \leftrightarrow SiOSi + H_2O \quad (8)$$

Water evaporates during both processes (7) and (8) [21–24]. Formed oxane bonds are presented on the right side of the Fig. 4 (a) [24]. The interaction of silanes with metal surface oxides is complicated process and depends on the substrate metal and its oxide [29]. SiOMe and SiOSi covalent bonds are assumed to form the excellent silane bonding to the metal surface [24]. SiOSi bonds can form already at room temperature, while SiOMe bonds need elevated temperature, i.e. curing of the silane layer [30]. As an example, 3-aminopropyltriethoxysilane (APS) layer after curing is presented in Fig. 4 (b) [31].

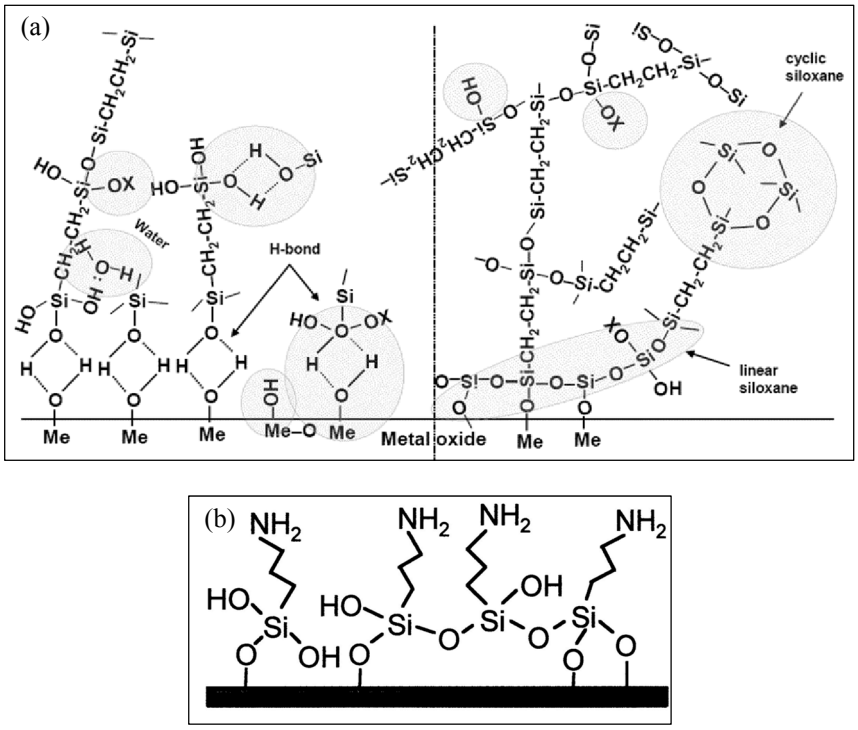

Figure 4. *Silane on metal substrates, (a) left side: silane bonding immediately after treatment with hydrogen-bonded interface, right side: silane bonding after condensation with covalent-bonded interface [24], (b) cured 3-aminopropyltriethoxysilane (APS) layer on substrate [31].*

Theoretically, on the substrate surface, silanes arrange themselves as high-degree-ordered monolayers which are influenced by the substrate surface [8,32]. However in practice, and especially in industrial applications, this kind of situation is not easy to produce because achieving the right-way arranged monolayer of silane is very difficult even at laboratory circumstances [32,33]. Franquet *et al.* presented a model to the possible bonding orientations of the aminosilane molecules on the metal surfaces; silanes can have three different bonding types: (1) bonding with the functional group, (2) with functional and silanol groups, or (3) with silanol groups. This model is presented in Fig. 5 [34]. As described earlier, the last one, bonding with silanol groups, is the most wanted to form good and stable adhesion with substrate.

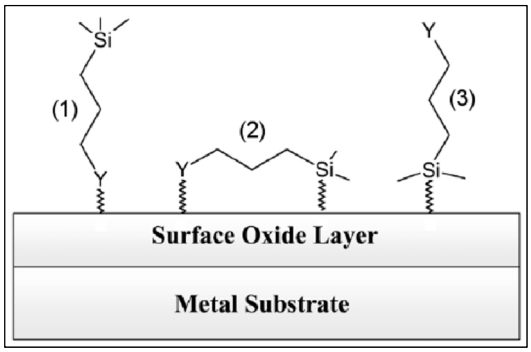

Figure 5. *Three different bonding orientations of aminosilanes with metals: (1) bonding with the functional group, (2) with functional and silanol groups, or (3) with silanol groups, modified from [34].*

Organofunctional groups at the ends of the silane chains can form bonds with organic materials. Bonding of silane to polymer is a complex process and it is dominated by the organofunctionality of silane and polymer characteristics. An example of the reaction between a silane-treated (APS) fiber and a polyvinyl chloride (PVC) matrix is presented in Fig. 6 [28].

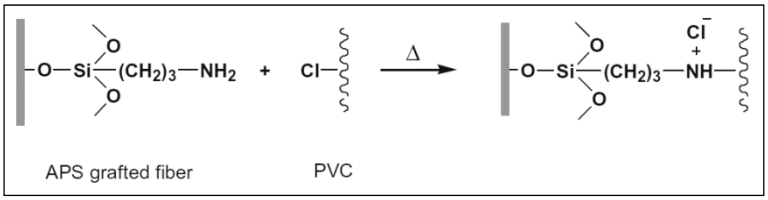

Figure 6. *Reaction between silane-treated (APS) fiber and polyvinyl chloride (PVC) matrix [28].*

2.2.3. Silane treatment

In silane treatment, the metal surface must be in contact with a silane solution having optimum concentration conditions for bonding. Silane can be deposited on the substrate by e.g. dipping or spraying, by chemical vapor deposition, or spin-on method [35]. The silane treatment consists of three steps: hydrolysis of silane, silanization of the substrate, and thermal curing of the silane-treated substrate. Processing steps related to the silane treatment can be divided to: metal cleaning, silane solution preparing, and silane layer growing. The parameters of the silane solution are: solution concentration, solution pH, and hydrolysis time. Parameters related to silane layer growth are: immersion time, curing time, and curing temperature [32].

At first, the silane has to be hydrolyzed to form reactive silanol groups to bond to the substrate. With functional trialkoxysilanes, the complete hydrolysis takes time from a few minutes up to few hours [23]. For example Bertelsen *et al.* noticed that the hydrolysis of γ-glycidoxypropyltrimethoxysilane (γ-GPS) completed in 30 minutes [25] while Abel *et al.* noticed that an optimum hydrolysis time for the same silane was one hour [26]. The hydrolysis time has to be long enough to complete the hydrolysis process but short enough to avoid

significant condensation reactions of the silanol groups. The functional groups of silane and solution pH affect the rate of hydrolysis [23].

Silane solutions used are usually very dilute (0.01–2 vol% silane) and solvent is usually distilled water or mixture of alcohol and distilled water and pH of the solution can be adjusted with e.g. acetic acid [8,21,22,24,25,32,36–38]. The thickness of the formed silane layer depends primarily on the silane solution concentration and it is almost independent on the immersion time of the substrate in the silane solution because silanol groups attach very rapidly to substrate [39]. Le Pen *et al.* noticed that a thicker silane layer (BTSE (bis-1,2-(triethoxysilyl)ethane) on aluminum) forms during drying the silane-treated substrate. Hence, the layer does not grow during dipping but when aluminum is removed from the BTSE solution; the viscous solution film is still on the aluminum surface and forms the layer within drying. Thus, the layer thickness depends only on the amount of BTSE on the metal surface after removing it from the solution. Therefore, the layer thickness increases linearly with the amount of BTSE in the solution and the thickness and evenness depend on the drying method and conditions. During the dipping, only few monolayers (0.5–2 nm) of BTSE are on the metal surface and they act as nucleation sites for the thicker layer within the drying step of the silane-treated aluminum substrate [37].

Thickness of the coupling agent layer is an important factor in the adhesion phenomenon. With too thin or thick layers, adhesion will suffer [7,36]. A thick layer can contain a chemical layer and a physical absorbed layer and a weak interface layer between them can decrease the adhesion strength. Thicker films can also become brittle [38]. However, the optimum thickness depends on bonded materials [7]. In our study, stainless steel-thermoplastic elastomer hybrids bonded with aminofunctional silane were characterized and the hybrids achieved the best peel strength values with the silane solution concentration of 0.5 vol% while with the concentrations of 0.1, 0.25, and 1.0 vol% the peel strength decreased. The silane layer thickness increased almost linearly by increasing the silane solution concentration and adhesion suffered with too thin or thick silane layer [36].

To achieve covalent SiOMe bonds, the silane layer should be cured at elevated temperature [30]. Chovelon *et al*. achieved the best adhesion results of the stainless steel-silane-epoxy system with curing temperatures between 100 and 150°C [40]. Abel *et al*. studied how long the cured γ-GPS layer was still active to form further well-bonded joint with plastic. They noticed that the activity started to decrease after the one week storage of the silane-treated substrate at 23°C in 50 % relative humidity [26].

2.2.4. Characterization of silane layer on metallic substrate

Silane layers on metal surfaces are usually characterized by: XPS, infra-red spectroscopy, and ellipsometry to determine layer thicknesses, elemental compositions, and chemical states. Jussila *et al.* studied adsorption of APS on stainless steel surface by XPS. They detected the formation of SiOSi, SiOMe, and –OH bonds at the oxide/silane interface and in addition, they noticed that the concentration of the hydroxyl groups on the stainless steel surface affected the bonding and morphology of silane layer; with high concentration, an APS monolayer with high degree of bonding was achieved [30]. Li *et al.* studied the chemical structure of γ-glycidoxypropyltrimethoxysilane (γ-GPS) on the low carbon steel surfaces [38] and Yuan *et al*. γ-aminopropyltriethoxysilane (γ-APS) on zinc surface by reflection-absorption infra-red spectroscopy [39]. They detected absorption bands like: SiOH, SiOSi, and NH_2 [38,39]. Yuan *et al*. detected with XPS that the amount of silicon in the γ-APS layer (from the solution concentration of 1 vol%) on the zinc surface was 4, 7, and 7 atomic% depending on the solution pH 4.5, 8, and 10.3, respectively [39]. While Li *et al.* studied the elemental distribution of the γ-GPS layer (from the solution concentration of 10 vol%) with an energy dispersive spectrometer (EDS) and they observed that the amount of silicon in the layer was 12, 76, and 31 atomic% depending on the curing temperature 100, 150, and 200°C, respectively [38]. Le Pen *et al.* studied BTSE on aluminum by e.g. spectroscopic ellipsometer to determine the layer thickness as the function of BTSE solution concentration. They noticed a linear relation between the layer thickness (about 100–450 nm) and the solution concentration (2–10 vol%) [37].

Previous characterization methods give numerical values about silane layers but it would be very important also to visualize them. However, for example cross-sectional electron microscopy studies about various silane layers on metal surfaces are almost lacking. Only few articles, to author's knowledge, about the electron microscopy of silanes on the metal surfaces have been published. Franquet *et al.* [34] and De Graeve *et al.* [41] studied the cross-sections of BTSE on aluminum with electron microscope. TEM studies of Franquet *et al.* observed that the BTSE layer was homogenous but its thickness varied much from 100 nm to 300 nm depending on the studied points on the substrate [34]. De Graeve *et al.* noticed similar features with FESEM [41]. BTSE is non-functional silane and therefore usually used for corrosion protection of the metal surface, not as an adhesion promoter in the metal-plastic hybrids. Altought, silane layers are widely studied, the detailed knowledge is still lacking due to the fact that silane is challenging for any characterization technique [32].

2.3. Metal surface pre-treatment

Substrate surface affects significantly silane layer formation. Rough or contaminated substrate surface can disturb the silane layer formation. A rough surface breaks up the first silane layer disturbing the formation of the second layer etc. [8]. Contaminants on the metal surface can block the active SiOH group reaction sites of the surface [42]. In addition the bonding of silane to metals is complicated process and depends also on metal and its oxide layer [29].

A uniform silane layer on the metal surface is required for optimal adhesion properties. However, producing even layers can be challenging [9–13]; non-uniform silane layers, deposited by dipping, on the copper and aluminum surface are presented in Fig. 7 [10,12].

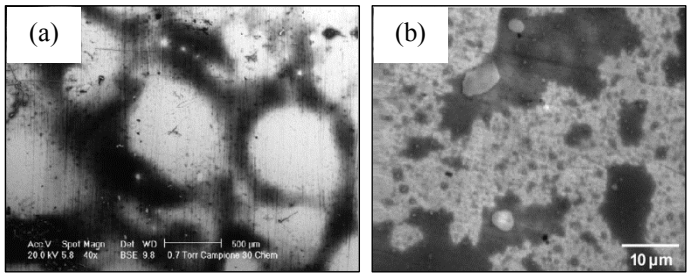

Figure 7. *Nonuniform silane layers on (a) copper, modified from [12] and (b) aluminum, modified from [10]. Dark areas correspond to silane.*

So prior to silane treatment, the surface pre-treatments for substrates are needed and the treatments have an important role in the joining processes. Surface pre-treatments for metallic substrates can be passive or active treatments. Passive surface pre-treatments remove contaminations and unfavourable layers from the metal surfaces. These methods can be e.g.: solvent wiping, vapor decreasing, abrasive cleaning, and chemical cleaning. Active surface pre-treatments change the substrate surface topography, chemistry, and oxide layer. They can be e.g.: acid etching, oxidizing, anodizing, and pickling. Various methods can be combined to achieve an optimal result [14,43]. The effect of various surface pre-treatments on the silane layer uniformity on the copper surface is presented in Fig. 8; nitric or sulphuric acid has no improving effect on the silane layer uniformity (Fig. 8 (a) and (b), respectively) but with alkaline solution treatment, better coverage is achieved (Fig. 8 (c)) [11].

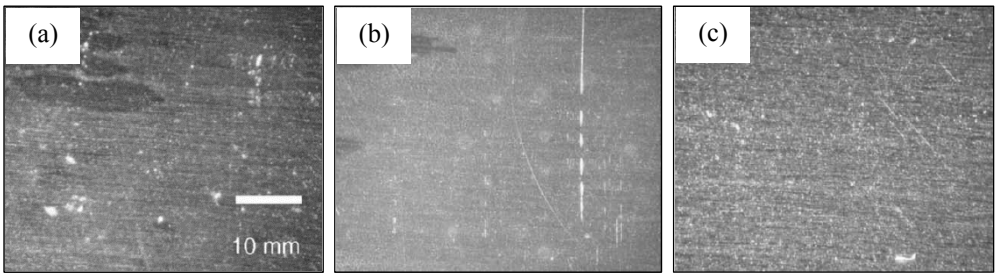

Figure 8. *Effect of surface pre-treatment on silane layer uniformity on copper, (a) nitric acid treatment, (b) sulphuric acid treatment, and (c) alkaline solution treatment. Dark areas correspond to silane [11].*

Susac *et al*. [9] and Kim *et al*. [10] tested active surface pre-treatments for aluminum alloy. Fresh, mechanically polished samples, followed by 20 hours of air-exposure, were used in Susac's *et al*. studies. They noticed that organosilane bonded poorly to a fresh, polished aluminum surface, and the existence of Al-Cu-Mg and Al-Fe-Cu-Mn-Si precipitates affected; silane bonded to the matrix but not to the precipitates. Silane bonded much better to an air-exposed surface than to a fresh sample, and its bonding to air-exposed aluminum was strongly influenced by the presence of Al-Cu-Mg and Al-Fe-Cu-Mn-Si precipitates [9]. Kim *et al*. studied the bonding of two organosilanes on aluminum alloy. They also studied the effect of oxidation treatment of aluminum on silane bonding. Samples were mechanically polished and then either exposed to air for 20 hours or oxidized in air at 200°C for 15 minutes. In the air-exposed surfaces, both the presence of Al-Cu-Mg and Al-Fe-Cu-Mn-Si precipitates and matrix affected the bonding, as in the studies by Susac *et al*. [9]. During the oxidation treatment at 200°C, oxides grew on the aluminum surface, and a uniform silane layer formed on the oxide layer [10].

2.4. Oxide structure on metal surface

Substrate surface, i.e. the oxide layer on it, influences the silane layer formation. Therefore, it is essential to have a good and detailed knowledge about the oxide structures on the metal surfaces. The oxidation of metals depends on the physical, chemical, and structural characteristics of the metal surface, as well as, on formed oxides, and oxidation conditions. The general equation for the chemical reaction in the oxidation of metal is [44]:

$$xMe + \tfrac{1}{2}yO_2 \leftrightarrow Me_xO_y \quad (9)$$

The classical theory of the oxidation of the metal surfaces at low temperatures by Cabrera and Mott describes that the oxide film grows as a uniform layer. At first, the oxide growth rate is very fast but with a layer thickness of about 2–10 nm it decreases. The driving force for oxidation is the electric-field-induced ionic transport which accelerates the initial oxidation but is rapidly attenuated with increasing oxide film thickness [45–47]. Nowadays, it is known that the theory of Cabrera and Mott is not correct. For example on the copper surface, the oxide film grows as oxide islands not as a uniform layer [46]. The oxidation of the metal surfaces usually consists of different steps: oxygen adsorption on the surface, initial fast oxidation, oxide nucleation and growth, and, finally, oxide film formation and its growth [44]. Schematic presentation of the initial oxidation stage of metal surfaces and the growth of the three-dimensional oxide layer are presented in Fig. 9 (a) and (b), respectively [48]. In the atmospheric environment, water always exists and thus the surface oxides of all common metals are modified by water adsorption resulting hydroxyl species (OH^-) on the metal oxides [14,48]. Regarding silane treatment, this is favourable as it ensures good bonding to the surface.

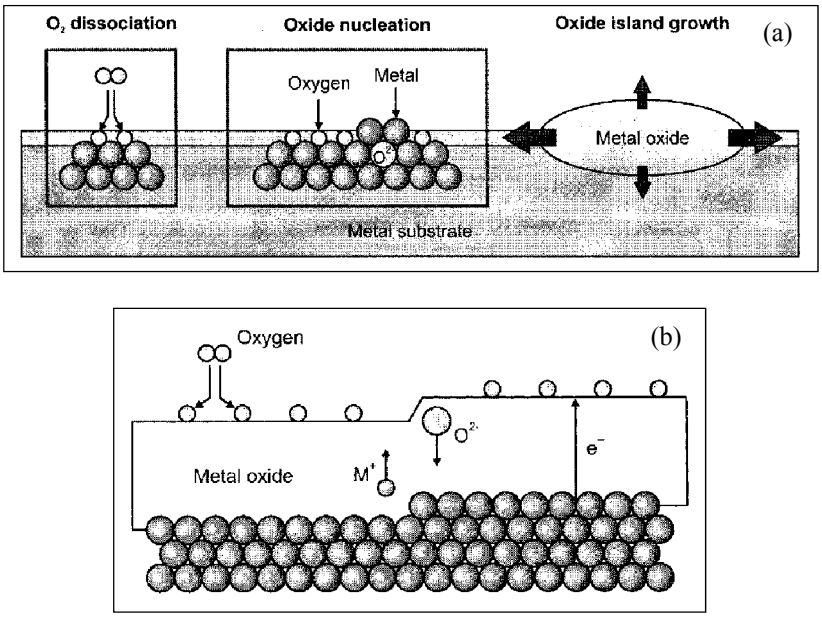

Figure 9. *Oxidation stages of metal surfaces, (a) dissociation and adsorption of O_2 onto metal surface, oxide nucleation, and oxide island growth, (b)* growth of three-dimensional oxide layer *[48].*

2.4.1. Oxide structure on stainless steel

Stainless steels are used in a wide range of different applications, from cutlery to food and chemical processing plants. This is due to the fact that they have very good corrosion resistance combined with excellent mechanical properties. Stainless steels are iron-based, chromium and nickel containing alloys; with minimum chromium content 10.5 weight%. “Stainless” is based on a thin and passive chromium oxide layer which forms spontaneously to the surface in the presence of oxygen. This layer is also self-preparing. Usually, stainless steels are divided into five groups: martensitic, ferritic, austenitic, duplex (ferritic-austenitic), and precipitation-hardening stainless steels. Martensitic stainless steels are ferromagnetic and their chromium content varies from 10.5 up to 18 weigth%. Their crystal structure is body-centered cubic (BCC) with a lattice parameter 0.287 nm. The chromium content of ferritic stainless steels varies from 10.5 up to 30 weigth%. Also they are ferromagnetic. Austenitic stainless steels have chromium content from 16 up to 26 weigth%. They are the most common stainless steels. Their structure is face-centered cubic (FCC) with a lattice parameter 0.359 nm. Their structure is achieved with austenite favouring elements like nickel, manganese, and nitrogen. Duplex stainless steels have ferritic-austenitic structure. Precipitation-hardening stainless steels are chromium-nickel alloys containing hardening elements like copper, aluminum, or titanium. They can have austenitic or martensitic structure. In addition of chromium and nickel, stainless steels can contain also other alloying elements, like aluminum, titanium, molybdenum, copper, and niobium [48–53].

Presence of oxygen is essential to the formation of the protective oxide layer on the stainless steel surface. It forms spontaneously in the presence of oxygen and protects stainless steel from the further oxidation [50]. At room temperature, a native oxide layer on stainless steel is typically 1–7 nm thick [54,55]. This is due to the fact that the mobility of the atoms and ions is insignificant and thus the growth of the oxide film stops. Further oxidation exists if, e.g. temperature increases or environment changes to chemically aggressive [56]. Many studies have indicated that oxide layers, formed on the stainless steel surfaces, have a complex, multi-layer structure. The layer consists of e.g.: Fe_2O_3, Fe_3O_4, FeO, and Cr_2O_3 [56–62]. The oxide layer just on the stainless steel/oxide interface is usually chromium-rich and the oxide layer above that is iron-rich [56]. The microstructural features of the oxide layer and growing of the oxide scale depend on many factors like: oxidation time, temperature, environment, and alloying elements [63]. At temperatures below 200°C, the formation of the oxide layer is driven by electro-migration so the thickness of the layer is independent from temperature. At higher temperatures, thermal diffusion becomes dominant and thickness increases with increasing temperature [55]. Oxide layers formed on stainless steel surfaces in atmospheric quantities of O_2 at room temperature and after heating in air at 400–600°C for one hour are presented in Fig. 10 (a) [61] and (b) [62], respectively.

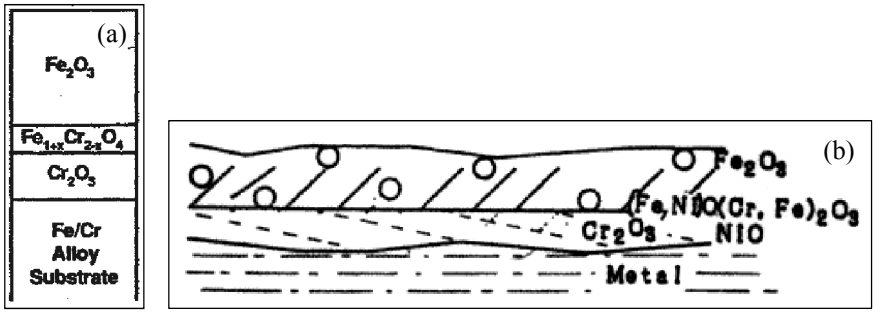

Figure 10. *Oxide layers formed on stainless steel surfaces (a) at room temperature [61] and (b) at 400–600°C [62].*

2.4.2. Oxide structure on copper

Copper and copper alloys are widely used because of their excellent electrical and thermal conductivity, good corrosion resistance, mechanical strength, and formability. They are used for example in: electronic, construction, heat transfer, and solar thermal applications. Copper grades with good electrical conductivity properties are e.g.: oxygen free copper (99.95 % Cu), silver bearing copper (99.90 % Cu, 0.04 % Ag), and phosphorus deoxidized copper (99.90 % Cu, 0.02% P). Copper can be alloyed also with other metals like: aluminum, nickel, zinc (brass), and lead (bronze). Pure copper has FCC structure with a lattice parameter 0.361 nm [64–67].

Copper is readily oxidized already at low temperatures and the formed oxide layers are not self-protective to prevent further oxidation. Depending on temperature, copper forms two thermodynamically stable oxides, Cu_2O and CuO or both [68–70]. The early stages of copper oxidation involve nucleation and growth of three-dimensional Cu_2O islands [46,71], the dominant mechanism in the island formation is surface diffusion [71,72]. The islands grow and coalesce and when the coalescence has occurred, the growth rate of the oxide layer decreases because the oxidation of the surface changes to the diffusion through the oxide layer [46]. At

room temperature, a native copper oxide layer is usually a few nanometers thick, consisting of Cu_2O and CuO [73,74]. S. Ghosh *et al*. noticed that at temperatures 30–150°C, Cu_2O was dominant oxide type but when temperature increased to 200°C and above, Cu_2O started to react with oxygen and CuO formed [75]:

$$2Cu_2O + O_2 \rightarrow 4CuO \quad (10)$$

According to Lahtonen's study, CuO starts to form from the surface to the bulk [76]. Cu_2O has a cubic structure with a lattice parameter 0.427 nm and CuO has a monoclinic structure with a lattice parameters: a ≈ 0.468 nm, b ≈ 0.343 nm, and c ≈ 5.12 nm [77].

Effect of alloying elements on the oxidation of copper is complicated and still not fully known. Zhu *et al*. studied the influence of impurities on the copper oxidation kinetics. They used 99.5 % and 99.9999 % pure copper specimens, and oxidation was carried out at 600–1050°C in 1 atm oxygen atmosphere. Based on their studies, in the case of high-purity copper, a thin and uniform CuO layer formed on the Cu_2O layer, and it was impervious to oxygen. Alloying elements can, however, cause porous and non-protective CuO layers and the increase the oxidation rate. On the other hand, alloying elements can slow down the initial stage of oxidation because alloying elements can impede the movement of copper atoms at the Cu_2O/Cu interface; thus the growth of Cu_2O nucleus becomes slower [78,79]. Also Lampimäki *et al*. noticed that the adsorption of O_2 induced segregation of Cu to the surface with Cu(Ag) alloy and that Ag had an inhibitive effect on the initial oxidation [80].

3. AIM OF PRESENT STUDY

The aim of the present study was to produce well-bonded metal-plastic hybrids with injection molding. The adhesion between metal and plastic was achieved with aminofunctional silane. However, the bonding of silane to as-received metal surface was poor, so active surface pre-treatments, i.e. polishing and oxidation, were needed. Manufacturing of the hybrids consisted of three steps: (1) the modification of the metal surface, (2) the silane treatment of modified metal, and (3) the injection molding of plastic onto the silane-treated metal. To optimize the parameters of each step, and hence to achieve well-bonded hybrids, the preforms of the hybrids were characterized after each manufacturing step. Atomic force microscopy, scanning electron microscopy, and transmission electron microscopy were the main characterization methods. This study consists of three publications related to the stainless steel-TPU hybrids and three publications related to the copper-TPU hybrids; the structure of the present study, the publications (I - VI), their main aims and findings, are presented in Fig. 11.

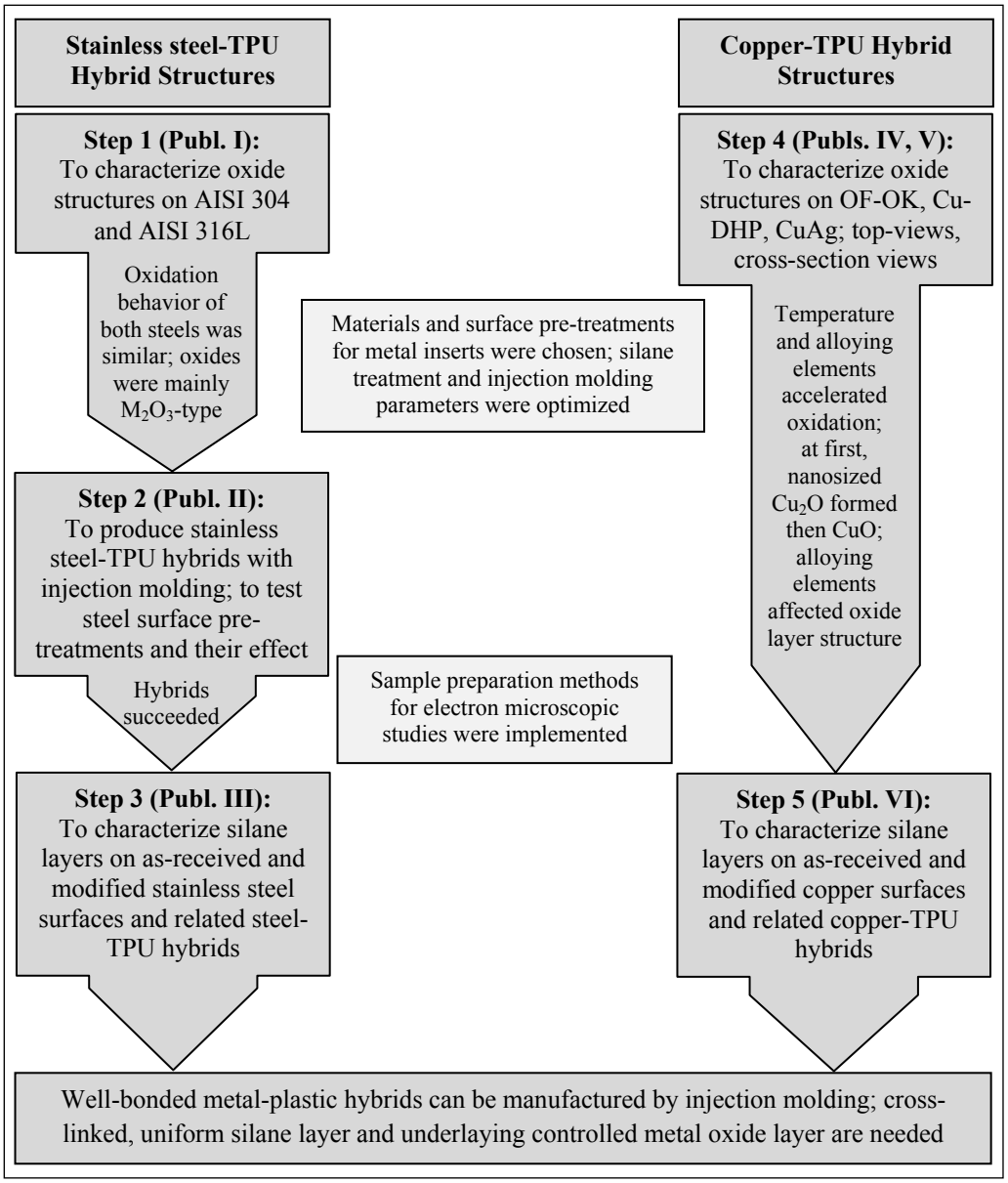

Figure 11. *Structure of present study; publications I-VI, their main aims and findings.*

4. EXPERIMENTAL PROCEDURES

In this chapter, studied materials are presented. Subsequently, the manufacturing process of the metal-plastic hybrids is introduced and finally, the characterization methods used after different manufacturing steps of the hybrids are described.

4.1. Materials

A metal-plastic hybrid contains a metal insert, an injection-molded plastic component, and a coupling agent layer between metal and plastic. Detailed description of the studied materials and their specific features are in this chapter including metals, silane, and plastic.

4.1.1. Metals

Stainless steel and coppers were used as insert materials in the studied metal-plastic hybrids. The metals were selected based on their relevance to novel hybrid components having either good corrosion properties or electrical conductivity. In addition, one reason to select copper was the fact that it has turned out to be a very challenging substrate material for hybrids, but having also many potential application areas in industry.

Stainless steels

Cr-Ni stainless steel (AISI 304) and Cr-Ni-Mo stainless steel (AISI 316L) from Outokumpu Stainless (Finland) were studied (publication I). They are austenitic stainless steels with FCC structure and with a lattice parameter of about 0.359 nm [48–50]. Designations and compositions of studied stainless steels are presented in Table 2 [81]. AISI 304 is the most commonly used stainless steel grade. It is used e.g. in chemical, paper, and food industry as well as in household wares and transportation [82]. AISI 316L, often called also as acid resistant steel, contains molybdenum which improves corrosion resistance in corrosive environments. They are used in many applications, e.g. in pulp & paper, textile, food, and medical industries [83]. The most commonly used stainless steel AISI 304 was chosen for further studies of the metal-plastic hybrids (publications II and III). The as-received AISI 304 plate used in this study was cold-rolled, heat-treated, pickled, and skin-passed. The surface was 2B finished with surface roughness (R_a) of 0.1–0.5 μm [84].

Table 2. *Compositions and designations of studied stainless steels [81].*

Designations			**Typical chemical composition [weigth%]**				
Outokumpu name	EN	ASTM	C	Cr	Ni	Mo	Fe
4301	1.4301	304	0.04	18.1	8.1	-	bal
4404	1.4404	316L	0.02	17.2	10.1	2.1	bal

Coppers

Oxygen-free copper (OF-OK), phosphorus deoxidized copper (Cu-DHP), and oxygen-free silver-alloyed copper (CuAg) from Luvata (Finland) were studied (publications IV and V). OF-OK (Cu min. 99.99 %, O_2 max. 10 ppm) has high electrical conductivity and due to that its typical applications are electrical applications, telecommunication cables, and printed circuits. Cu-DHP (Cu min 99.90 %, P 150–400 ppm) is used as building and construction material because it has excellent formability and weldability. Silver in copper increases softening temperature and due to that, typical applications of CuAg (Cu+Ag min. 99.98 %, Ag 0.03 %, O_2 max. 10 ppm) are e.g. commutators for small motors and graphic plates for the engraving industry [65]. Studied CuAg was not a standard CuAg grade because its silver content was as high as 1 weigth%. Copper materials were in cold rolled condition with the reduction of 80–90 %. The microstructure of the cold rolled material was heterogeneous and therefore, more homogeneous microstructures for the oxidation treatments were produced by recrystallization treatment. The recrystallization temperature for each copper grade was defined by annealing the samples at different temperatures for two hours and measuring the resulting Vickers-hardness values. Based on these studies, the recrystallization temperature for OF-OK was selected as 350°C, for CuAg 225°C, and for Cu-DHP 450°C. The average grain size of all copper samples after recrystallization was 5 μm.

OFE-OK and Cu-DHP were chosen for the further studies of the copper-plastic hybrids (publication VI). OFE-OK is similar to OF-OK but OFE-OK has lower O_2 content (Cu min. 99.99 %, O_2 max. 5 ppm). OFE-OK has a high electrical conductivity and therefore its main applications are in the field of printed circuits, bonding applications, electrical conductors, magnetrons, vacuum interrupters, and tubes [65]. Copper grades, OFE-OK and Cu-DHP, for metal-plastic hybrid applications were received from Luvata in normal cold rolled surface quality. The grains were isotropic and stable under testing conditions so no recrystallization treatment was carried out.

4.1.2. Silane

Coupling agent used in the present study was amino-functional N-(β-aminoethyl)-γ-aminopropyltrimethoxysilane (γ-AEAPS, commercially available as Dow Corning Z-6020, Dow Corning, USA) with chemical formula:

$$NH_2(CH_2)_2NH(CH_2)_3Si(CH_3O)_3 \quad (11)$$

This coupling agent has hydrolysable methoxy groups to react with metals and an amino group to bond with plastics. Estimated molecular weight is 222 g/mol and its reactivity matches well with acrylic, nylon, epoxy, phenolics, PVC, melamines, urethanes, and nitrile rubber [85]. In the very initial studies also other silanes were tested. The best peel strength values of the metal-plastic hybrids were achieved, however, with γ-AEAPS. Without silane, no adhesion between as-received or modified metals and plastic was achieved.

4.1.3. Plastic

Plastic in the injection-molded metal-plastic hybrids was thermoplastic urethane (TPU, commercially available as Estane GP 85 AE nat, Lubrizol Advanced Materials Inc., USA). TPU has good durability, abrasion and wear resistance, and low temperature flexibility. It can be used e.g. in overmold grips, tool handles, seals and gaskets, cable jackets, fuel system components, and sporting good components [86].

4.2. Manufacturing of metal-plastic hybrid

Manufacturing process of the metal-plastic hybrids consisted of three steps: (1) surface modification of metal, (2) silane treatment of metal, and (3) injection molding of plastic onto silane-treated metal. Below, various manufacturing steps are described in detail.

4.2.1. Oxidation treatments for stainless steel and copper

Prior to silane treatment, the surface modifications, i.e. electrolytical polishing and oxidation, for metals were carried out. At first, the metal surfaces were electrolytically polished to achieve a clean and smooth surface for further oxidation treatments. The stainless steel surfaces were electrolytically polished by JaloteräsStudio (Finland) while the copper surfaces were electrolytically polished by using nitric acid in methanol (1:2 as volume fraction) at temperature of -50°C.

Electrolytically polished stainless steel and copper surfaces were oxidized in air in a ceramic tube furnace to achieve controlled oxide layers. Electrolytically polished stainless steel specimens were oxidized at 350°C for 5, 100, and 300 minutes and copper specimens at 200°C for 25 minutes. Also other temperatures and exposure times were studied (publications I, IV, and V) but they resulted in unacceptable surface quality for future processing. The above mentioned treatments were chosen for metal-plastic hybrid processing.

As-received metals with industrially finished surfaces were used as reference surfaces in the metal-plastic hybrids to compare the effect of the surface modifications on the formation of the silane layers and on the adhesion strengths of the hybrids. Prior to silane treatment, the as-received metal surfaces were cleaned with acetone and ethanol in ultrasonic cleaner for six minutes. Metals and related surfaces with surface roughness values (R_a) used in the metal-plastic hybrids are presented in Table 3.

Table 3. *Metals and related surfaces with surface roughness values (R_a) used in studied metal-plastic hybrids.*

Metal	Surface	R_a [nm](*)
AISI 304	As-received (industrially finished, cleaned)	66
	Electrolytically polished (JaloteräsStudio)	19
	Electrolytically polished + 5 min oxidized at 350°C	14
	Electrolytically polished + 100 min oxidized at 350°C	6
	Electrolytically polished + 300 min oxidized at 350°C	25
OFE-OK	As-received (industrially finished, cleaned)	72
	Electrolytically polished (at laboratory)	7
	Electrolytically polished + 25 min oxidized at 200°C	8
Cu-DHP	As-received (industrially finished, cleaned)	44
	Electrolytically polished (at laboratory)	13
	Electrolytically polished + 25 min oxidized at 200°C	11

(*)Surface roughness values (R_a) calculated from atomic force microscope images (13 µm x 13 µm), see section *4.3.1. Atomic force microscopy* in page 21.

4.2.2. Silane treatment

Various silane treatment parameters for stainless steel were studied in paper [36]. According to the results, the best peel strength values for stainless steel-plastic hybrids were achieved with the silane solution concentration of 0.5 vol%. This concentration was used in the stainless steel-TPU hybrids (publications II and III). The silane solution concentrations of 0.25 and 0.5 vol% were used for coppers (publication VI).

The silane solutions were used at their natural pH 9–10 and deionized water was used as the solvent. The solution was stirred for one hour. This is sufficient time for hydrolysis to form active silanol groups [23,25,26]. After hydrolyzation, the samples were dipped in the solution for 5 minutes. The curing of the silane layers was performed in air at 110°C for 10 minutes using specimen tilting of 30° from the horizontal plane. This angle ensured the flow off of the excess silane solution from the specimen surface.

4.2.3. Injection molding

Insert injection molding process was used to manufacture metal-plastic hybrids. The injection molding was carried out next day after the silane treatment, i.e. the surface of the silane layer was still active to form bonds with plastic [26]. The hybrids were processed with an injection molding machine (Fanuc Roboshot αC30, Japan). In the injection molding process, the silane-treated metal insert was placed in the mold and then, TPU is injection-molded on the insert and after cooling time (15 seconds), the finished hybrid structure was removed from the mold. The size of the metal inserts used was 100 mm x 12 mm x 0.5 mm and the thickness of the injection-molded plastic component was about 2 mm. Injection molding parameters are presented in

Table 4 and the schematic presentation of the finished hybrid part is presented in Fig. 12; thickness of the metal insert with oxide layer was 0.5 mm and a 2 mm thick TPU layer and a silane layer between them.

Table 4. *Injection molding parameters.*

Speed (injection)	20 mm/s
Temperature (mold)	50°C
Back pressure	750 bar, 3 s
Cooling time	15 s
Plastization	50 rpm, 10 bar
Temperature (cylinder)	200 - 195 - 190 - 185 - 35°C

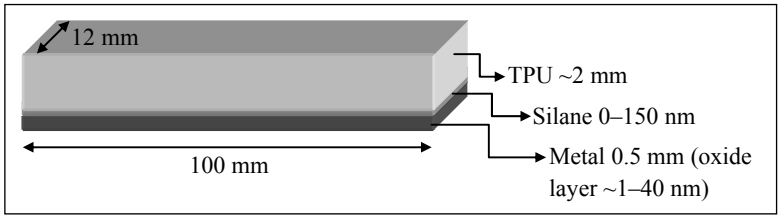

Figure 12. *Schematic presentation of finished injection-molded metal-plastic hybrid.*

4.3. Characterization

The hybrids were characterized after every manufacturing step. Characterization methods used were: atomic force microscopy (AFM), scanning electron microscopy (SEM), transmission electron microscopy (TEM), reflection absorption infrared spectroscopy (RAIRS), X-ray photoelectron spectroscopy (XPS), and peel test.

4.3.1. Atomic force microscopy

The oxide layers on the electrolytically polished AISI 304 and AISI 316L surfaces were studied with atomic force microscopy (AFM, Dimension 3100, Nanoscope IVa, Veeco Instruments Inc., USA) in Optoelectronics Research Centre at Tampere University of Technology (TUT) (publication I). The tapping mode with a scan rate 0.5 Hz was used.

Oxide layers on the electrolytically polished copper surfaces, silane layers on the various metal surfaces, and the peeled surfaces of the metal-plastic hybrids were studied with AFM (Nanoscope E AFM/STM, Veeco Instruments Inc., USA) in Department of Materials Science at TUT (publications II, III, IV, and VI). A pyramidal probe and a 200 μm long triangular silicon nitride cantilever were used with a spring constant of 0.12 N/m. Both contact and constant force modes were used. Surface roughness values (R_a) were calculated from AFM images with the software Nanoscope (R) III.

4.3.2. Scanning electron microscopy

The silane layers, finished metal-plastic hybrids, and the peeled surfaces of the hybrids were studied with scanning electron microscopes (SEMs). In the studies of the publication II, SEM XL 30 (Philips, the Netherlands) equipped with energy dispersive X-ray spectrometer (EDS, DX-4, EDAX, USA) was used. In the publications III and VI, field-emission scanning electron microscope (FESEM) Zeiss ULTRAplus (Carl Zeiss SMT AG, Germany) was used. It is equipped with inlens secondary electron (SE) and angular selective backscatter (AsB) detectors and EDS (INCA Energy 350 EDS analyzator with INCAx-act detector, Oxford Instruments, UK).

Conventional metallographic cross-sectional sample preparation for SEM studies turned out to be unsuitable for the silane-treated stainless steel or copper because silane reacted with sample preparation resin. Bending the samples in liquid nitrogen, like described in [41], was nor successful because of the silane layer did not become brittle enough. So, the simple sample preparation method was implemented [87]: the silane-treated metal surface was glued with carbon glue on an aluminum SEM stub and with a surgical blade an incision was produced through the silane layer. In the edges of the incision, the silane layer detached from the substrate and the cross-sections of the layers could be characterized. The image of the silane-treated metal substrate, glued on the SEM stub, with incisions is presented in Fig. 13 (a). The cross-section samples from the finished hybrid parts were prepared with conventional metallographic method. The samples from the peeled surfaces were glued on aluminum SEM stub and further carbon-coated.

4.3.3. Transmission electron microscopy

The oxide layers and silane layers on the metal surfaces were studied with transmission electron microscope (TEM, JEM-2010, Jeol, Japan) equipped with EDS (Noran Vantage with Si(Li) detector, Thermo Scientific, USA). The oxide layers were studied from both top- and cross-section-views and silane layers were mainly studied from cross-section-view.

Electrolytically polished TEM samples were used for oxidation treatments to study the top-views of the oxide layers on metals (publications I and V). The polishing was carried out with a twin jet electrolytical polisher (Tenupol 5, Struers, Denmark) using a solution of nitric acid in methanol (1:2 as volume fraction) at -50°C. Pre-thinning prior to polishing was made mechanically with SiC-papers to 0.1 mm thickness and then 3 mm diameter discs were cut with a disc punch (Model 310, South Bay Technology Inc., USA) from the pre-thinned samples. The fresh sample was studied with TEM and further it was oxidized with various exposure times and the sample was characterized within every exposure time. The same area and orientation of the fresh and related oxidized sample was located in TEM. The image of the top-view TEM sample is presented in Fig. 13 (b).

The cross-sectional TEM samples of the oxidized or silane-treated metals (publications I, III, V, VI) were prepared as follows (based on [88]): small pieces of the samples, oxidized / silane-treated coppers / stainless steels, were cut to size ~1.5 mm x 1 mm x 0.4 mm, the pieces were attached oxide layers / silane layers face-to-face to a titanium grid by carbon glue and the grid was pre-thinned by hand to the thickness of ~100 µm and then with a dimple grinder (Model 656, Gatan Inc., USA) to the thickness of ~20 µm. The final thinning was made with a precision ion polishing system (PIPS, Model 691, Gatan Inc., USA). The image of the cross-sectional TEM sample is presented in Fig. 13 (c).

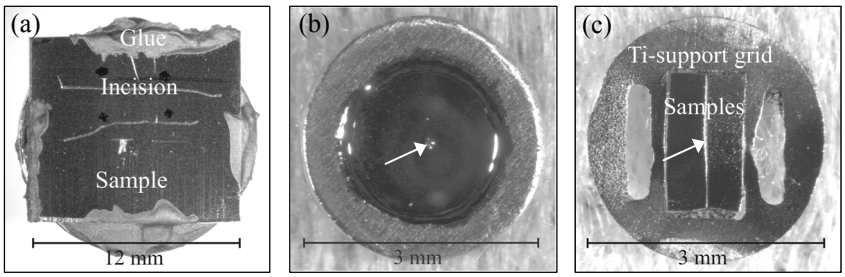

Figure 13. *Images of FESEM and TEM samples, (a) FESEM sample of metal substrate with silane layer; sample glued on SEM stub and incisions produced by surgical blade, (b) top-view TEM sample with perforation (marked with arrow) prepared by electrolytical polishing, and (c) cross-sectional TEM sample with perforation (marked with arrow) in Ti-support grid prepared by mechanical thinning.*

4.3.4. X-ray photoelectron spectroscopy

Chemical analysis of the AISI 304 surfaces was performed by X-ray photoelectron spectroscopy (XPS, XSAM 800, Kratos Analytical, UK) in Surface Science Laboratory at TUT employing non-monochromated Al *Kα* radiation (photon energy = 1486.6 eV). The as-received and oxidized stainless steel surfaces were investigated before and after silanization (publication III). Spectra were recorded at normal emission geometry using fixed retarding ratio mode for survey spectra (retarding ratio = 20) and fixed analyzer transmission mode for narrow scan spectra (pass energy = 38.0 eV). Base pressure during the measurements was below 1×10^{-8} mbar. The chemical states of elements were determined from XPS spectra by least-squares fitting of Gaussian-Lorentzian lineshapes with a Shirley type background to the main photoelectron peaks. The analysis was carried out using CasaXPS software (version 2.3.13) [89]. All binding energy values were referenced to the Fe $2p_{3/2}$ peak (707.0 eV for metallic Fe and 711.2 eV for Fe_2O_3) [90], because the commonly used C 1*s* peak may shift as much as 1 eV between silanes and carbonous impurities [30].

4.3.5. Reflection absorption infrared spectroscopy

The copper surfaces before and after silane treatments (publication VI) were characterized with reflection absorption infrared spectroscopy (RAIRS, Optics Tensor 27, Bruker, Germany with Veemax II reflection unit, Pike Technologies, USA). The angle used was 70°, scan number 128, and resolution 4 cm^{-1}. Sample size was 25 mm x 30 mm, so a circular mask with the diameter of 5/8" was used. Background spectrum was collected using gold-plated mirror and 128 scans. The chemical compositions of the peeled sample surfaces (copper sides) were studied also with RAIRS. The angle used was 40° and mask size 3/8" (sample size 100 mm x 11 mm) otherwise the device and parameters were as above.

4.3.6. Peel test

The peel strength values of the injection-molded metal-plastic hybrids were measured using 180° peel test (publications II, III, and VI). Samples were conditioned before testing at 23±1°C in 50±2 % relative humidity for 72 hours. A testing machine (Messphysik, Austria) with a 1 kN load cell and 100 mm/min crosshead speed was used. To determine failure types, peeled sample surfaces were studied with an optical stereomicroscope (Leica MZ 7.5, Switzerland), AFM, FESEM, and RAIRS.

Summary of characterization methods

As a conclusion of the experimental part, the manufacturing steps of the metal-plastic hybrids and characterization methods within every manufacturing step are presented in Fig. 14.

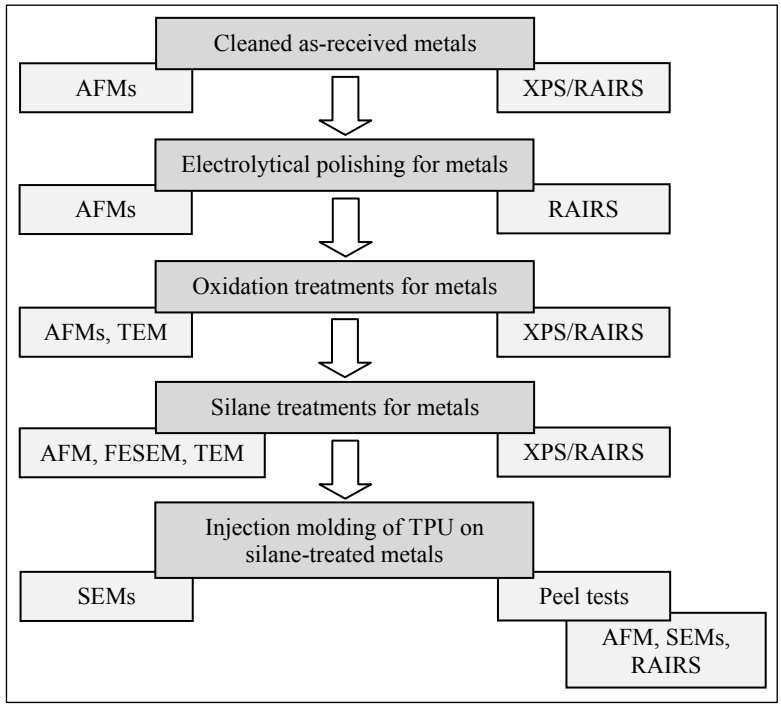

Figure 14. *Manufacturing steps of metal-plastic hybrids and characterization methods after each step.*

5. RESULTS AND DISCUSSION

The aim of this study was to produce well-bonded metal-plastic hybrid structures by injection molding. The adhesion between metal and plastic was produced by aminofunctional silane. The bonding of silane to the as-received metal surfaces was poor so prior to silane treatment, the metal surfaces were modified by electrolytical polishing and oxidation treatments to improve the silane bonding. The metal surfaces, as-received and modified, were characterized before silane treatments with AFM, TEM, RAIRS, and XPS. Silane layers on the as-received and modified metal surfaces were studied with AFM, FESEM, TEM, RAIRS, and XPS. The finished metal-plastic hybrid parts were studied with peel tests and further with AFM, FESEM, and RAIRS. In the following, the main results of the attached six original publications are presented and discussed.

5.1. Stainless steel-TPU hybrid

Stainless steel-plastic hybrids would have many applications for example in automotive and household industry offering e.g. savings in weight and costs, part reduction, corrosion properties, and better dimensional stability. Nowadays in industrial hybrid structures, adhesion is mainly based on mechanical interlocking. In this study, chemical adhesion between stainless steel and thermoplastic urethane was produced with aminofunctional silane. The condition of the stainless steel surface affected the formed silane layer, and this in turn to properties of the hybrid.

5.1.1. Oxide structure on stainless steel

The silane bonding on the as-received stainless steel surface was poor. Therefore, active surface pre-treatments, i.e. electrolytical polishing and oxidation, were studied to improve silane layer formation on the stainless steel surface. The oxidation treatments of AISI 304 and AISI 316L were carried out in air at 350°C for 5, 25, 100, and 300 minutes. The oxide layers were characterized with AFM, TEM, and XPS.

Topographies of the oxide layers on the AISI 304 surface were studied with AFM; the images of the polished and oxidized stainless steel surfaces are presented in Fig. 15 [Publication I]. In atmosphere, stainless steels form a thin, passive oxide film fast and spontaneously [50,54] so the polished surface had a thin native oxide layer. The AFM image of the fresh sample indicated also some oxide islands in the native oxide film (Fig. 15 (a)). During 5 minutes (Fig. 15 (b)) and 25 minutes (not shown) exposures, number of these oxide islands increased and after 100 minutes (Fig. 15 (c)) and 300 minutes (Fig. 15 (d)) exposures, the islands had combined forming a continuous layer on the native oxide layer. Topography of the oxide layer changed between 100 and 300 minutes exposure resulting flat islands after 100 minutes and the pointed-shape of the islands after 300 minutes exposure [Publication I].

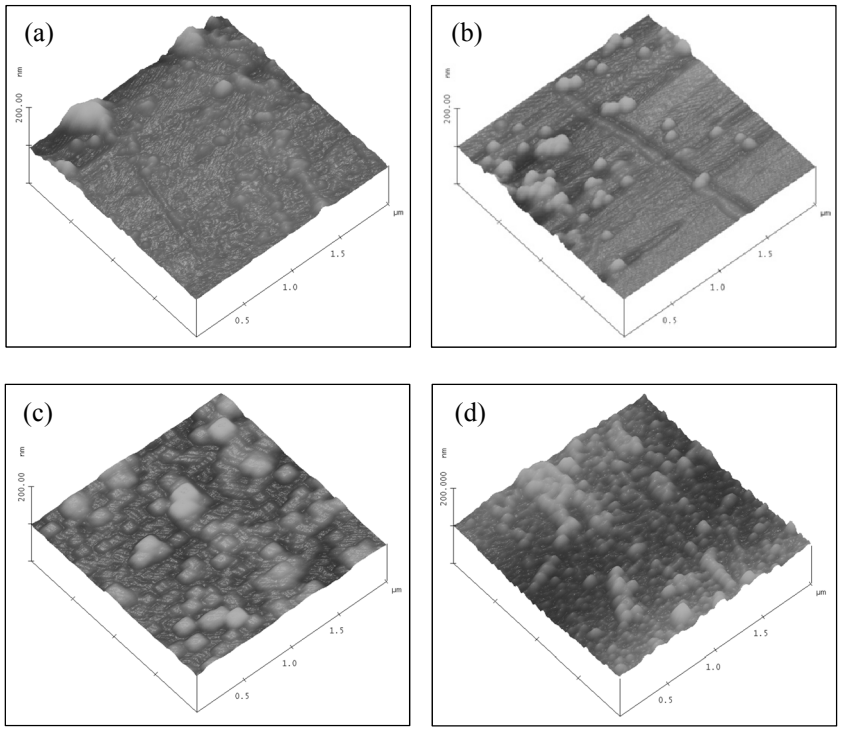

Figure 15. *AFM images of AISI 304, (a) electrolytically polished, (b) oxidized in air at 350°C for 5 minutes, (c) for 100 minutes, and (d) for 300 minutes. Scanned area x = y = 2 µm and z = 200 nm [Publication I].*

Topographical changes of the oxide layers, due to the exposure time, can be better observed by AFM section analyses (Fig. 16). According to them, during 5 and 25 minutes exposures, single about 18 nm high and 200 nm wide islands formed on the native oxide layer (Figs. 16 (a) and (b)). The amount of the islands and hence the surface roughness increased between 5 and 25 minutes exposure. After 100 minutes oxidation the islands covered the surface and they formed a flat, uniform layer (Fig. 16 (c)) while during 300 minutes, pointed-shape islands formed (Fig. 16 (d)) [Publication I]. According to AFM studies, an optimal stainless steel surface for silane treatment and hence for metal-plastic hybrid applications would be after oxidation treatment in air at 350°C for 100 minutes resulting in a uniform and flat oxide layer.

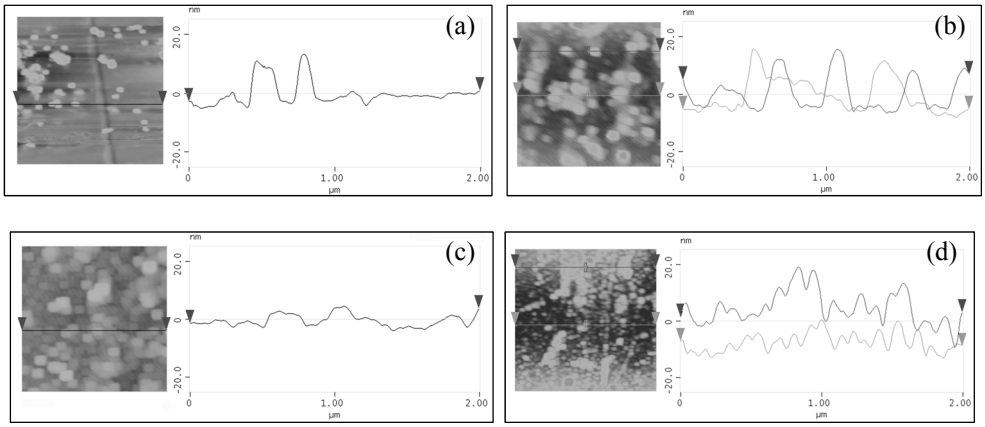

Figure 16. *AFM section analyses of AISI 304 oxidized in air at 350°C for (a) 5 minutes, (b) 25 minutes, (c) 100 minutes, and (d) 300 minutes. Scanned area x = y = 2 µm and z = ± 20 nm [Publication I].*

Cross-sectional TEM samples were prepared from 100 and 300 minutes oxidized stainless steels; images are presented in Figs. 17 (a) and (b), respectively. The oxide layers were dense and their thicknesses after 100 minutes exposure was ~15 nm and after 300 minutes ~18 nm. The selected area electron diffraction (SAED) pattern of 100 minutes oxidized AISI 304 is presented in Fig. 17 (c). The SAED pattern is from the top-view TEM sample so, the spots are originated from the underlying stainless steel grain (**B** = [112]). Based on the SAED pattern, the structure of the nanocrystalline oxide layer was mainly of type M_2O_3 [Publication I]. The lattice plane spacing values (d) of e.g. Cr_2O_3 (rhombohedral structure, a ≈ b ≈ 0.495 nm and c ≈ 1.36 nm [91,92]) and Fe_2O_3 (rhombohedral structure, a ≈ b ≈ 0.503 nm and c ≈ 1.37 nm [92,93]) are very close to each other and therefore, exact identification of the oxide structures with the ring pattern was not possible. According to the cross-sectional TEM images, the oxide layers were very uniform and no multilayer structures were detected. According to AFM and TEM studies, the oxidation of AISI 304 and AISI 316L started rapidly, during 5 minutes, but when a protective oxide layer was formed, the oxidation rate decreased and the thickness of the layer was almost same after 100 and 300 minutes exposures. Thus, the formed oxide layers were protecting stainless steels from further oxidation [Publication I].

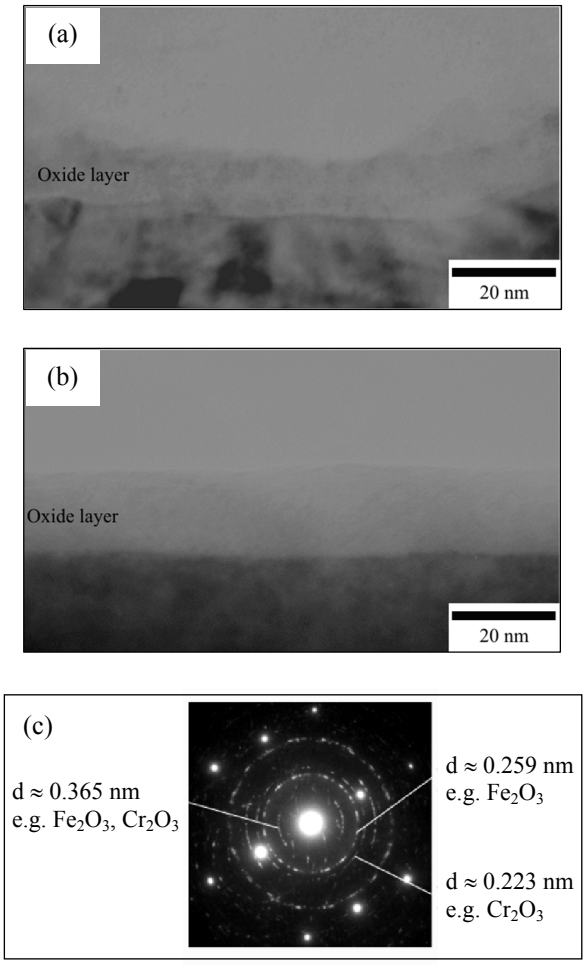

Figure 17. *Cross-sectional TEM images of (a) AISI 316L oxidized in air at 350℃ for 100 minutes and (b) AISI 304 oxidized in air at 350℃ for 300 minutes. (c) SAED pattern of oxidized (in air at 350℃ for 100 minutes) AISI 304 (top-view), d values of some rings marked and also possible oxide structures with these values, spots originated from underlying stainless steel grain (**B** = [112]) [Publication I].*

Chemical analysis of the AISI 304 surfaces (as-received and 100 minutes oxidized) was performed by XPS. The XPS survey spectra indicating the elements present on the as-received and oxidized AISI 304 surfaces are presented in Fig. 18 (a) and narrow scan spectra and identification of chemical states from C 1*s* and O 1*s* transitions are in Figs. 18 (b) and (c), respectively. Relative concentrations of the chemical species are presented in Table 5. According to the analysis results, the cleaned as-received surface consisted of the stainless steel alloy (metallic Fe and Cr) and a thin surface oxide film (Fe and Cr oxides and hydroxides) that were largely covered by carbonous impurities (organic compounds containing C–C and C=O type bonds). Ca, N, and F due to the pickling process were detected as trace elements. The surface oxide was a typical passive layer on stainless steel, i.e., it was ~1–3 nm thick and enriched with Cr oxides but did not contain any Ni [54]. Electrolytical polishing and further oxidation treatment produced an oxide layer consisting of mainly Fe_2O_3 at the outermost

surface. This result agrees well with the literature e.g. [56,62]. In addition, the amount of C from surface impurities was reduced considerably from 59.6 atomic% to 17.4 atomic% as a result of the treatment. Mn, Ca, P, and Zn were detected as trace elements on the polished and oxidized surface. Both surfaces contained an appreciable amount of hydroxyl species resulting from reactions with ambient water, which is required for the efficient bonding of silanes [Publication III].

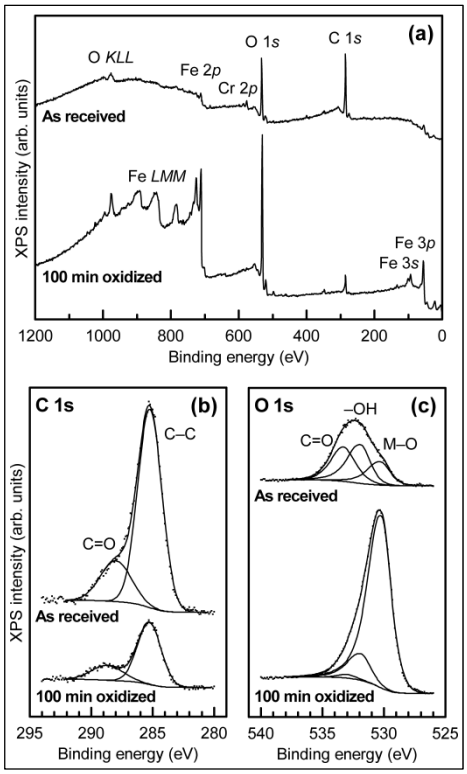

Figure 18. *XPS spectra, (a) XPS survey spectra, (b) C 1s spectra, and (c) O 1s spectra obtained from as-received and 100 minutes oxidized AISI 304 surfaces [Publication III].*

Table 5. *Relative concentrations of chemical species (in atomic%) on as-received and 100 minutes oxidized stainless steel surfaces as determined by XPS. The bulk composition of AISI 304 stainless steel is included for reference [Publication III].*

	Fe (met)	Fe (ox)	Cr (met)	Cr (ox)	Ni (met)	C (C-C)	C (C=O)	O (M-O)	O (-OH)	O (C=O)
Bulk alloy	73.0		19.2		7.6					
As-received	0.6	1.7	0.2	1.9	-	47.2	12.4	8.7	14.3	13.1
100 min oxidized	-	12.9	-	0.4	-	13.2	4.2	59.4	9.1	0.9

XPS studies indicated that the outermost layer (XPS signal comes mainly from the depths 0–5 nm [69]) of the oxide after 100 minutes oxidation at 350°C was mainly Fe_2O_3 [Publication III] which agrees well with TEM results that the oxide layer is M_2O_3-type [Publication I]. In general, oxidation behavior of both AISI 304 and AISI 316L was very similar and differences in oxide structures were not observed. Based on that, the most commonly used stainless steel AISI 304 was chosen as a metal insert for further studies on metal-plastic hybrids because it can be proposed that AISI 316L behaves similarly in those applications. Subsequently, the oxidation treatments in air at 350°C for 5 and 100 minutes were chosen as active surface modifications prior to silane treatment to improve silane bonding to the stainless steel surface. With 100 minutes exposure, a uniform, dense, smooth, ~15 nm thick M_2O_3-type oxide layer was achieved. Also 5 minutes exposure was chosen as a surface pre-treatment for AISI 304 because the short exposure time would save the manufacturing time of the stainless steel-plastic hybrids and the oxidation of the AISI 304 surfaces started already during 5 minutes exposure [Publication I].

5.1.2. Silane layer on stainless steel

Stainless steel AISI 304 was used as a metal insert in the stainless steel-TPU hybrids. Surface conditions used were: (1) cleaned, industrially finished (publications II and III), (2) electrolytically polished (publication II), (3) electrolytically polished and oxidized in air at 350°C for 5 minutes (publications II and III), (4) electrolytically polished and oxidized in air at 350°C for 100 minutes (publications II and III), and (5) electrolytically polished and oxidized in air at 350°C for 300 minutes (publication II). Industrially finished as-received stainless steel insert was used as a reference surface to study the effect of the surface modifications on the silane layer formation. According to the oxidation studies of the stainless steel surfaces [Publication I], the most potential oxidation treatment for stainless steel substrate, prior to silane treatment, is in air at 350°C for 100 minutes. However, the oxidation of the stainless steel surface started already during 5 minutes exposure and also that oxidation treatment would be interesting because it would save the manufacturing time of the stainless steel-plastic hybrids. Initial studies were carried out with electrolytically polished stainless steel insert (with native oxide layer, without oxidation treatment) and with long-time oxidized (in air at 350°C for 300 minutes) stainless steel insert. The peel strength values of the hybrids manufactured with these surface conditions were lower than with 5 and 100 minutes oxidized stainless steel inserts [Publication II]. This was probably due to the rough surface of the oxide layer formed after 300 minutes exposure compared to the oxide layers formed after 5 and 100 minutes oxidation (Figs. 15 and 16) while the rough surface disturbed the formation of the silane layer and hence decreased the peel strength values of the related hybrid structures. In addition, the smooth surface produced by electrolytical polishing but with native oxide layer was not suitable for hybrid applications. Therefore, the oxidation treatments in air at 350°C for 5 and 100 minutes were chosen as active surface pre-treatments for stainless steel insert for further study in the publication III and the as-received surface was used as reference.

Silane layers on the as-received and oxidized (in air at 350°C for 5 / 100 minutes) AISI 304 surfaces were produced from the silane solution concentration of 0.5 vol%. Silane layers were characterized with AFM, FESEM, TEM, and XPS. During the silane treatment, two different silane layer areas formed on the oxidized stainless steel surfaces in the transverse direction of the insert: the middle area of the insert with a thick silane layer and the edge areas with a thin silane layer. The schematic drawing, bottom-end-view, of the formed silane layer on the polished and oxidized stainless steel surface with thicker middle area and thinner edge areas in the transverse direction of the insert is presented in Fig. 19. This kind of effect was not detected on the as-received surface [Publication III].

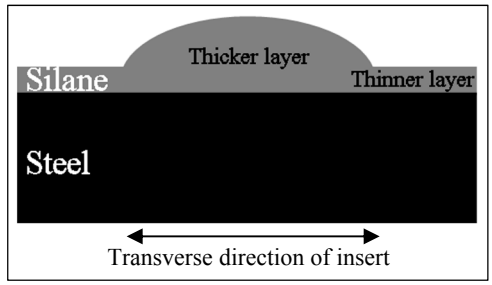

Figure 19. *Schematic drawing of formed silane layer on oxidized stainless steel surface: thick silane layer in middle area and thin layer in edge areas, modified from [Publication III].*

The topographies of the stainless steel surfaces before and after silane treatment were studied with AFM. The images of the as-received and oxidized stainless steel surfaces with and without silane are presented in Figs. 20 (a) and (b), respectively. On the as-received stainless steel surface, silane existed mainly in the grain boundaries (Fig. 20 (a)). While, on the oxidized stainless steel surface, the silane layer totally covers the oxide structure (Fig. 20 (b)); silane covered the oxide structure in the both areas, with a thick and thin silane layers, in the transverse direction of the insert. The industrially finished as-received surface is much rougher compared to the modified surfaces and therefore, the scanned area of the images of the as-received surface is larger than that of the modified surfaces [Publication III].

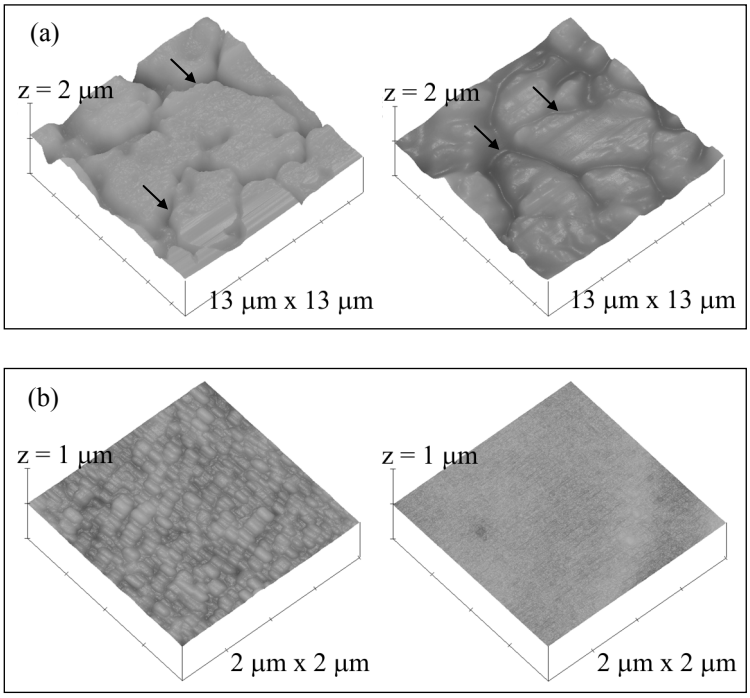

Figure 20. *AFM images of stainless steel surfaces with and without silane, (a) as-received stainless steel before and after silane treatment, respectively; grain boundaries marked with arrows and (b) 100 minutes oxidized stainless steel before and after silane treatment, respectively. Notice different x-, y-, and z-scales in (a) and (b) [Publication III].*

Thickness and uniformity of the silane layers on the stainless steel surfaces were studied with FESEM and TEM. The images of the thick and thin silane layers on the 100 minutes oxidized stainless steel insert are presented in Fig. 21. According to FESEM and TEM results, the silane layer thickness is very different between the middle area with thickness of 150 nm (Figs. 21 (a) and (b)) and the edge areas with thickness of 20 nm (Figs. 21 (c) and (d)). The SAED pattern of the silane layer is presented in Fig. 21 (b), indicating the amorphous structure of the layer. According to FESEM and TEM studies, the silane layers were very similar on the both 5 and 100 minutes oxidized stainless steel surfaces. On the as-received stainless steel surface, the silane layer thickness varied much between grains and grain boundaries (not shown). In the grain boundaries, the layer thickness was about 100 nm and on the grains varied from 0 up to 10 nm. The situation was similar through the whole insert and differences between the middle and edge areas were not detected with the as-received stainless steel insert. The silane layer was even on all stainless steel surfaces in the longitudinal direction. This indicates that the selected curing angle of 30° produces uniform silane layer in the longitudinal direction. However, the thickness varied more on the as-received surface due to grain boundaries while with the oxidized stainless steel inserts, the silane layer thickness varied only between the middle area and the edge areas in the transverse direction but inside these areas, the layer thickness was very even [Publication III].

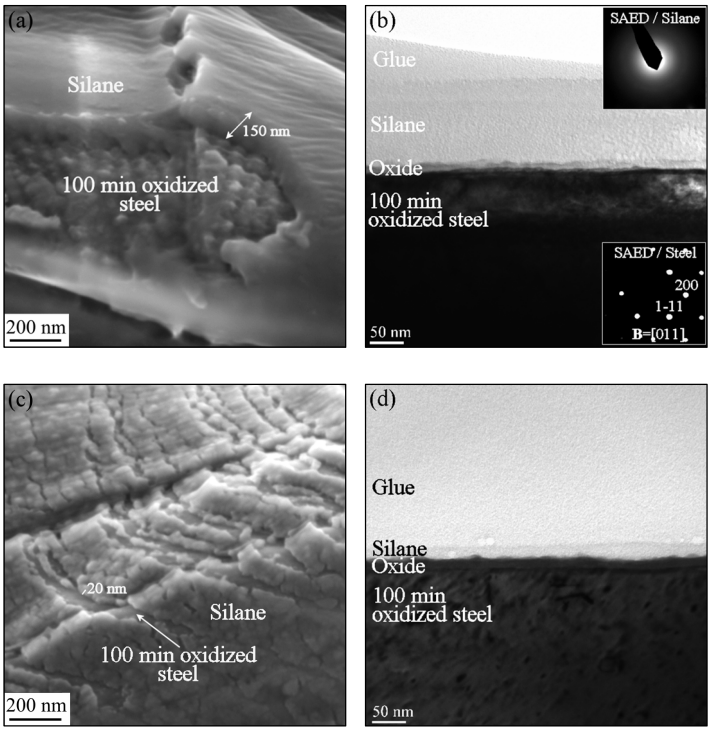

Figure 21. *FESEM and TEM images of silane layers on electrolytically polished and 100 minutes oxidized stainless steel surface, (a) FESEM and (b) TEM image of middle area of insert in transverse direction with thick silane layer (150 nm), (c) FESEM and (d) TEM image of edge area in transverse direction with thin silane layer (20 nm) [Publication III].*

In order to determine the chemical composition of the produced silane layers and to evaluate their quality in this respect, XPS analyses were carried out for silane-treated as-received and 100 min oxidized stainless steel inserts. Moreover, samples of both thin and thick silane layers on the 100 minutes oxidized surface (edge and middle areas) were analyzed [Publication III]. The information depth was ~8 nm from the outermost surface (three times the inelastic mean free path value of photoelectrons in silane materials) [30]. Survey spectra obtained from the surfaces after silanization are presented in Fig. 22 (a) and narrow scan spectra of the C 1*s* and O 1*s* transitions are in Figs. 22 (b) and (c), respectively. Relative concentrations of chemical species are presented in Table 6. The results were consistent with the formation of silane layer on top of stainless steel, indicated by the appearance of Si 2*p* (103.2 eV) and N 1*s* (400.6 eV) signals from the silane as well as attenuation of the Fe 2*p* and O 1*s* (M–O) signals from the substrate, with less attenuation in the case of a thin silane layer. The N 1*s* peak position was characteristic of amino type species (e.g. $–NH_2$), indicating no reaction of the aminofunctional groups during the preparation of the layer. So, the aminofunctional groups were available at the top of the silane layer to react further with plastic. The C 1*s* (C–C) signal originating from silanes was shifted towards higher binding energies (up to 286.3 eV) in comparison to that from carbonous impurities. In addition, the O 1*s* component related to siloxane bonds (Si–O–Si, at 533.1 eV) increased in intensity. However, this component still included some contribution from C=O type species due to atmospheric impurities (CO_2, CH_2O, etc.) [94], as indicated by the C 1*s* spectra (the component at 288 eV). No further impurities apart from those originally present on the stainless steel surfaces were detected. The main differences between the as-

received surface and 100 minutes oxidized surfaces were apparent, as indicated in Table 6. Firstly, the silane coverage obtained on the as-received surface was considerably less than on the oxidized surface, as seen from the relative concentrations of Si. On the other hand, the C/Si ratio was very high on the silane-treated as-received stainless steel surface, indicating that the surface was still largely covered by carbonous impurities, whereas on the 100 minutes oxidized surface the ratio was closer to the value of pure γ-AEAPS. Thus, the presence of impurities on the as-received surface seemed to hinder the formation of a uniform silane layer, but this issue was remedied by the polishing and oxidation pre-treatment. Concerning subsequent utilization of the silanized surfaces, the amount of N (amino) species needed for the bonding of plastic was also favorable on the 100 minutes oxidized surface [Publication III].

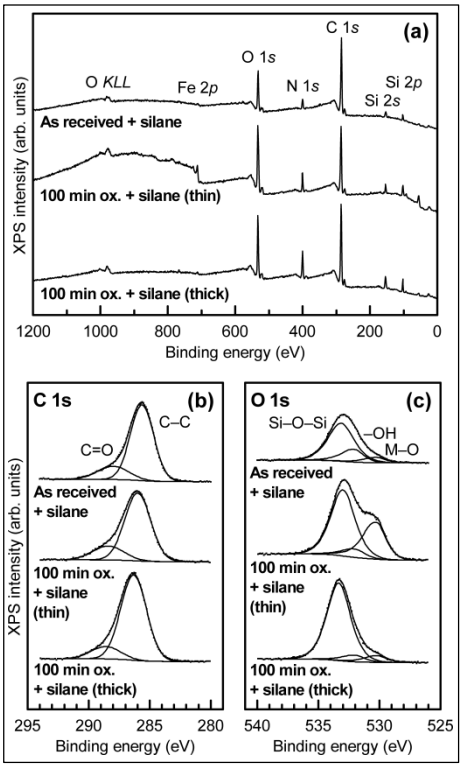

Figure 22. *XPS spectra, (a) XPS survey spectra, (b) C 1s spectra, and (c) O 1s spectra obtained from silane-treated as-received and 100 minutes oxidized stainless steel surfaces. In case of 100 minutes oxidized surface, spectra corresponding to thin silane layer at edge of insert and to thick silane layer in middle of insert are shown [Publication III].*

Table 6. *Relative concentrations of chemical species (atomic%) on as-received and 100 minutes oxidized stainless steel surfaces after silane treatment as determined by XPS. Ideal composition of fully hydrolyzed and condensed γ-AEAPS is included for reference. Calculated ratio of C to Si is also indicated [Publication III].*

	Fe (ox)	Cr (ox)	C (C–C)	C (C=O)	O (M–O)	O (–OH)	O (Si–O–Si)	N	Si	C/Si ratio
γ-AEAPS			52.6				15.8	21.1	10.5	5.0
As-received	0.3	0.4	54.7	12.7	1.9	4.5	15.1	5.4	4.8	14.0
100 min oxidized (thin)	1.9	-	40.6	10.0	10.1	2.3	18.4	10.0	6.7	7.5
100 min oxidized (thick)	0.3	-	49.3	8.2	1.7	1.7	20.5	9.9	8.4	6.9

5.1.3. Hybrid structure

Cross-sectional FESEM samples of the injection-molded hybrids were prepared to find out the effects of the injection molding on the silane layer. The sample preparation was very challenging and for example in the case of the hybrid manufactured with the as-received stainless steel insert, TPU easily detached from the stainless steel surface and secondly, metal easily penetrate into the smoother silane layer during metallographic sample preparation. Cross-sectional FESEM image of the stainless steel-TPU hybrid with 100 minutes oxidized stainless steel insert from the middle area of the insert (in both transverse and longitudinal directions) is presented in Fig. 23. The silane layer thickness is about 200 nm and its bonding to the stainless steel surface is good without any cracks or pores [Publication III].

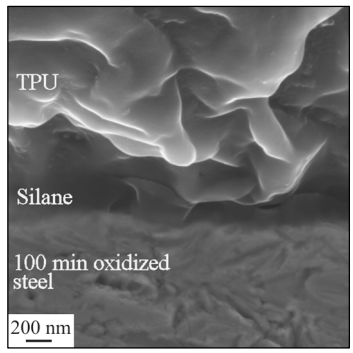

Figure 23. *Cross-sectional FESEM image of stainless steel-TPU hybrid [Publication III].*

The adhesion strengths of the stainless steel-TPU hybrid structures were measured with peel test. The peel strength values of the hybrids manufactured with different surface finishes of the stainless steel inserts are presented in Fig. 24. The stainless steel surface, before silane treatment, had a significant effect on the formed silane layer and hence the peel strength of the related hybrid structure. The surface modifications improved the adhesion strength of the hybrids compared to the hybrids manufactured with as-received stainless steel insert. On the cleaned as-received stainless steel surface, a rough and contaminated surface disturbs the silane layer formation resulting in a nonuniform layer with slight amount of N (amino) species to react with plastic causing poor adhesion strength of the hybrid [Publication III]. According to literature, a rough surface breaks up the first layer disturbing the formation of the second layer [8] and contaminants block the active sites of the surface to react with silanols [42]. A flat surface with Fe_2O_3-layer produced by 100 minutes oxidation treatment resulted in a thin, uniform silane layer with more N (amino) species to react with plastic achieving well-bonded stainless steel-TPU hybrids [Publication III]. Even if the electrolytically polished stainless steel surface, without oxidation treatment, is smooth, a native oxide layer with Fe and Cr oxides is not enough to form a uniform silane layer and hence well-bonded hybrid structures. In the hybrid manufactured with 300 minutes oxidized stainless steel, the formed oxide layer was too rough (Figs. 15 and 16) to form uniform silane layer decreasing thus the peel strength values [Publications I, II].

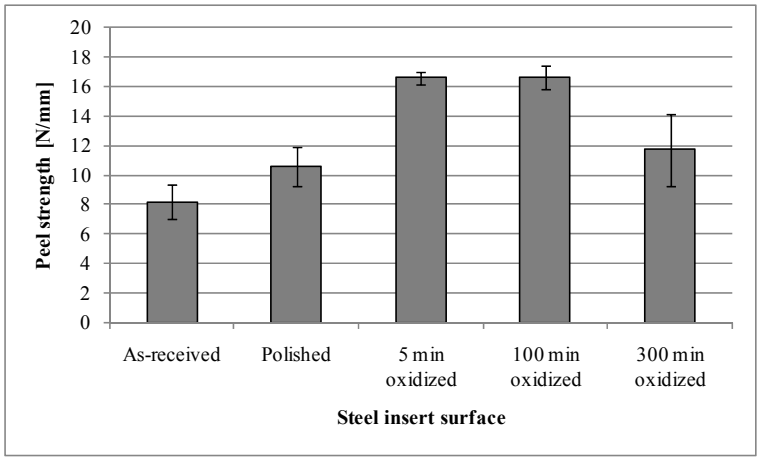

Figure 24. *Peel strength values of stainless steel-TPU hybrid structures manufactured with various surface finishes of stainless steel inserts, results combined from publications II and III.*

The peeled surfaces, metal and plastic sides, of the hybrids manufactured with as-received and 5 / 100 minutes oxidized stainless steel hybrids were studied with FESEM and AFM to clarify failure types. Various failure types, cohesive in TPU, adhesive in silane/TPU interface and failure inside the silane layer, were detected. According to the FESEM studies, the hybrids manufactured with 5 or 100 minutes oxidized stainless steel inserts failed similarly and the stainless steel sides were covered by TPU except the middle area of the insert with thick silane layer. So, the failure in the edge areas of the insert with thinner silane layer (20 nm) was totally cohesive in TPU and it was the dominating failure type. FESEM image of the peeled stainless steel side (100 minutes oxidized) from the edge area of the insert in the transverse direction with thin silane layer is presented in Fig. 25 (a); the stainless steel surface is totally covered by TPU. The stainless steel side from the boundary area between the thin and thick silane layer is presented in Fig. 25 (b) where the failure type changes from failure inside the silane layer or adhesive failure in silane/TPU interface (with thick silane layer) to totally cohesive failure in TPU (with thin silane layer) [Publication III].

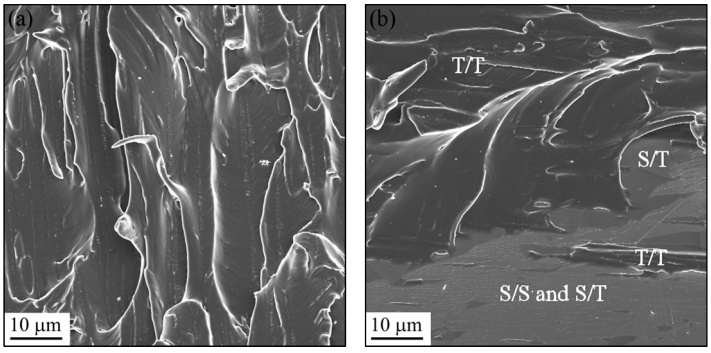

Figure 25. *FESEM images of peeled surface, stainless steel side, of injection-molded hybrid manufactured with 100 minutes oxidized stainless steel from (a) area with thin silane layer and (b) boundary area between thin (top of image) and thick (bottom of image) silane layer. S/S is failure in silane layer, S/T is adhesive failure in silane/TPU interface, and T/T is cohesive failure in TPU [Publication III].*

FESEM and AFM images of the peeled stainless steel side (5 minutes oxidized) from the middle area of the insert in the transverse direction with thicker silane layer (150 nm) are presented in Fig. 26. In the area, few TPU islands were visible on the stainless steel side showing cohesive failure in TPU (T/T in Fig. 26 (a)). The failure also existed as adhesive in silane/TPU interface (S/T in Fig. 26 (a), (b), and (c)). In this area, the top of the silane layer (Fig. 26 (c)) was as smooth as after silane treatment indicating that its bonding with TPU was poor. However, in the thick silane layer area, the failure mainly existed inside the silane layer (S/S in Figs. 26 (a) and (b)). It can be concluded from the FESEM studies showing that the electrolytically polished and 5 minutes oxidized stainless steel surface without silane layer (Fig 26 (d)) had not surface structure as in Figs. 26 (b) and (c), so the failure did not happen in the stainless steel/silane interface but inside the silane layer. In the silane/silane failure areas, most of the silane layer was detected in TPU side (not shown) indicating that silane/silane failure happened very close to the stainless steel surface [Publication III]. According to literature, a thick silane layer can contain chemically and physically bonded layers and a weak interface layer between them can decrease the adhesion strength [38] and it is possible that the failure existed between those two layers inside the silane layer in the case of the thick (150 nm) layer. The hybrid manufactured with as-received stainless steel insert had no differences between

middle area and edge areas in the transverse direction (not shown); no cohesive failure in TPU was detected and the failure inside the silane layer dominated what was expected based on the discontinuous silane layer formation and low peel strength values [Publication III].

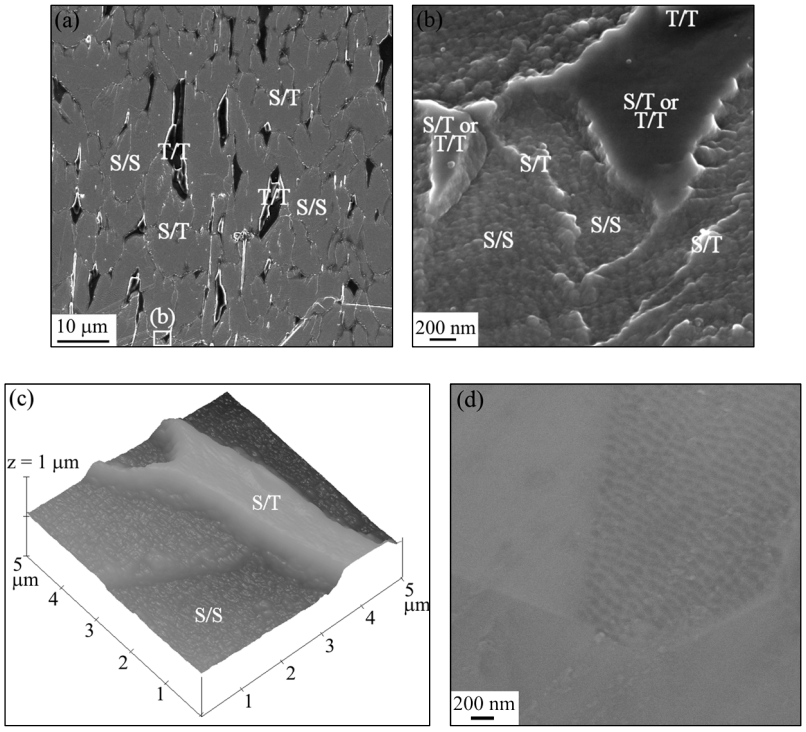

Figure 26. *Peeled surfaces, stainless steel side, of injection-molded hybrid manufactured with 5 minutes oxidized stainless steel insert from middle area of insert with thick silane layer, (a) and (b) FESEM images and (c) AFM image. S/S is failure in silane layer, S/T is adhesive failure in silane/TPU interface, and T/T is cohesive failure in TPU [Publication III]. (d) As comparison, FESEM image of 5 minutes oxidized stainless steel surface.*

5.2. Copper-TPU hybrid

Copper-TPU hybrids would be useful for example in the electrical and constructional applications offering e.g. saving in weight, part reduction, good electrical and thermal conductivity, and faster assembly. In this study, chemical adhesion between copper and thermoplastic urethane was produced with aminofunctional silane. The bonding of silane to copper surfaces, and hence adhesion between copper and plastic, was improved with pre-treatments, i.e. electrolytical polishing and oxidation, of the copper surfaces. The condition of the copper surfaces affected the formed silane layer and this in turn to the properties of the hybrid.

5.2.1. Oxide structure on copper

The silane bonding to the as-received copper surface was poor so, active surface pre-treatments, electrolytical polishing and oxidation treatment, were used to improve silane bonding to the copper surfaces. The oxidation treatments of recrystallized, electrolytically polished OF-OK, Cu-DHP, and CuAg were carried out in air at 200°C for 25 and 100 minutes and at 350°C for 5, 25, and 100 minutes. The oxide layers on the coppers were studied with AFM, TEM, and RAIRS.

Topographies of the copper surface before and after oxidation treatments at 200 and 350°C were studied with AFM. The images are presented in Fig. 27; according to AFM studies, the roughness of the copper surfaces increased with exposure temperatures and times [Publication IV].

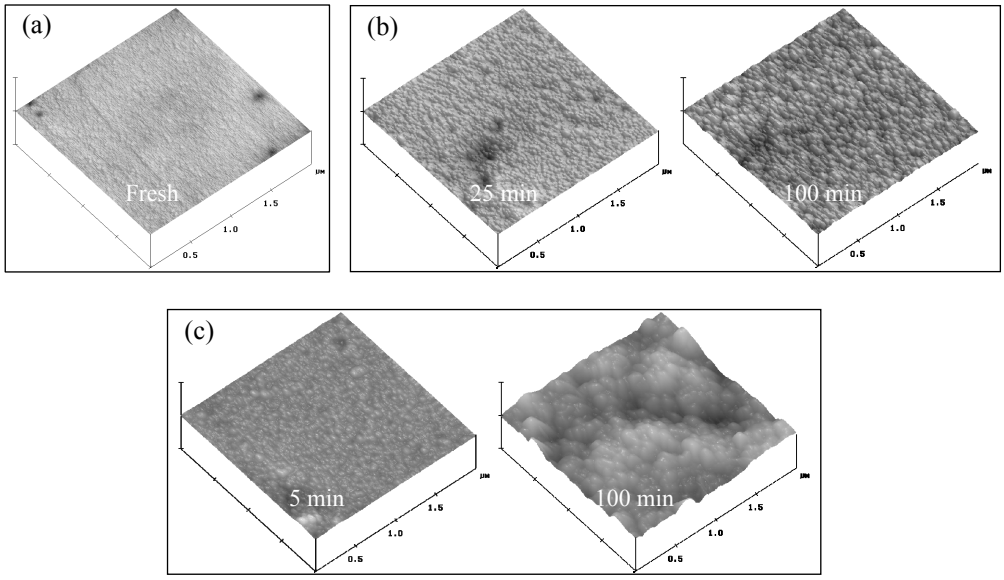

Figure 27. *AFM images of OF-OK, (a) electrolytically polished, fresh surface, (b) oxidized in air at 200°C for 25 and 100 minutes, and (c) oxidized at 350°C for 5 and 100 minutes. Scanned areas x = y = 2 µm and z = 500 nm [Publication IV].*

The cross-sections of the oxide layers were studied with TEM. The images of OF-OK, CuAg, and Cu-DHP after 25 minutes oxidation at 200°C are presented in Figs. 28 (a)–(c) and the SAED pattern from the oxide layer is presented in Fig. 28 (c). The SAED patterns of all samples were similar indicating a nanocrystalline Cu_2O layer (d values correspond closely to cubic Cu_2O with a ≈ 0.427 nm [77,95]). The oxide layers were dense and their average thicknesses after 25 minutes oxidation at 200°C were 40–50 nm [Publication V]. In the further copper-plastic hybrid studies, OFE-OK was used as the metal insert. Also its oxide layer was analyzed indicating similar nanocrystalline, ~40 nm thick Cu_2O layer as in OF-OK, Cu-DHP, and CuAg [Publication VI].

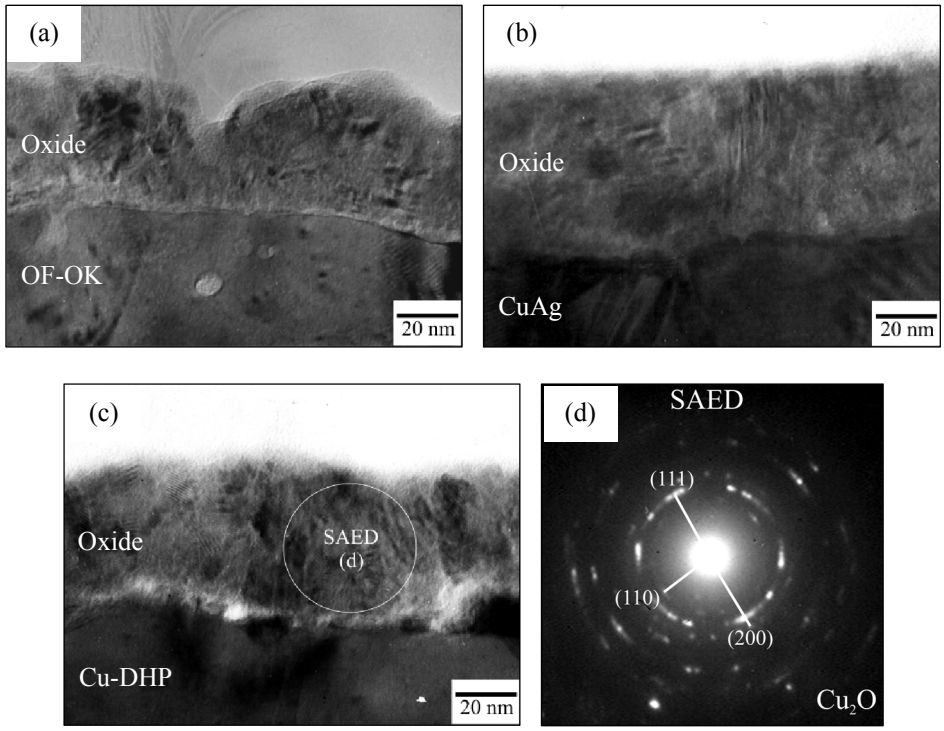

Figure 28. *Cross-sectional TEM images of (a) OF-OK, (b) CuAg, and (c) Cu-DHP after 25 minutes oxidation in air at 200℃, (d) SAED pattern from oxide layer of Cu-DHP [Publication V].*

According to cross-sectional TEM studies, after 100 minutes oxidation at 200°C, a nanocrystalline Cu_2O layer formed on all studied copper surfaces. The oxide layer and especially its surface on OF-OK was much denser than that of CuAg and Cu-DHP. The average thickness of the oxide layer on OF-OK was 100 nm, and that on CuAg and Cu-DHP 120–150 nm. This indicates that at longer exposure times the oxidation rate of alloyed coppers, CuAg and Cu-DHP, is faster than that of unalloyed copper, OF-OK. After 5 minutes oxidation at 350°C, the situation was very similar to that after 100 minutes oxidation at 200°C; a nanocrystalline, ~80 nm thick Cu_2O layer formed on all studied coppers [Publication V].

The cross-sectional TEM images of OF-OK, CuAg, and Cu-DHP after 25 minutes oxidation at 350°C are presented in Figs. 29 (a)–(c), respectively, and SAED pattern from the innermost oxide layer is presented in Fig. 29 (d). All studied samples had a similar innermost 300–400 nm thick Cu_2O layer, but the oxide layer on it was different depending on the copper grade. In the case of unalloyed OF-OK, about 300 nm thick CuO layer (monoclinic structure with lattice parameters: $a \approx 0.468$ nm, $b \approx 0.343$ nm, and $c \approx 5.13$ nm [77]) with circular-shaped grains grew on the Cu_2O layer. While, 600–800 nm thick layer consisting of columnar-shaped Cu_2O and CuO grains grew onto the Cu_2O layer of alloyed Cu-DHP and CuAg. Cu_2O and CuO grains were identified by electron diffraction. SAED patterns of the different oxide grains are presented in Figs. 30 and 31. In the publication V, more detailed diffraction studies are presented. Typical interface between Cu_2O and mixed oxide grains (Cu_2O and CuO) containing layer in either alloyed CuAg or Cu-DHP is presented in Fig. 32. TEM studies indicated that oxidation rate of alloyed coppers was generally much faster than that of unalloyed OF-OK and that the alloying elements (Ag and P) formulated thicker, larger, and mixed copper oxide grain structure [Publications IV and V]. This agrees well with literature, indicating that alloying elements can slow down the initial stage of oxidation but may later on cause formation of non-protective CuO layers [78,79].

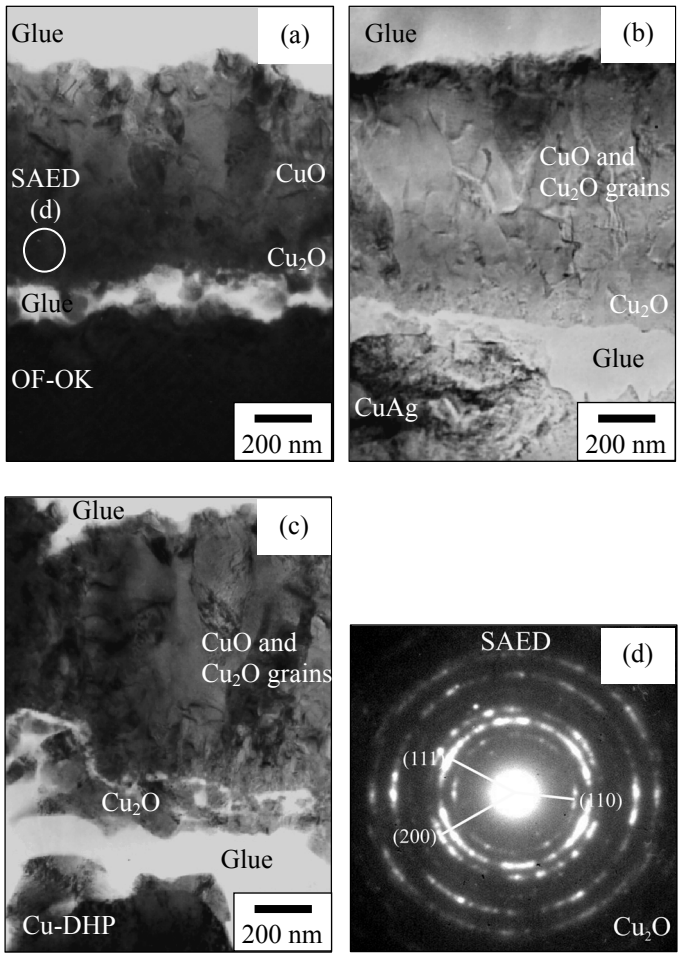

Figure 29. *TEM images of (a) OF-OK, (b) CuAg, and (c) Cu-DHP after 25 minutes oxidation in air at 350℃ and (d) SAED pattern taken from innermost oxide layer of OF-OK, modified from [Publication V].*

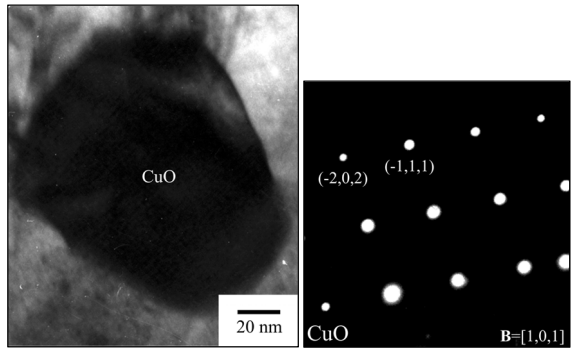

Figure 30. *CuO grain of OF-OK and its SAED pattern [Publication V].*

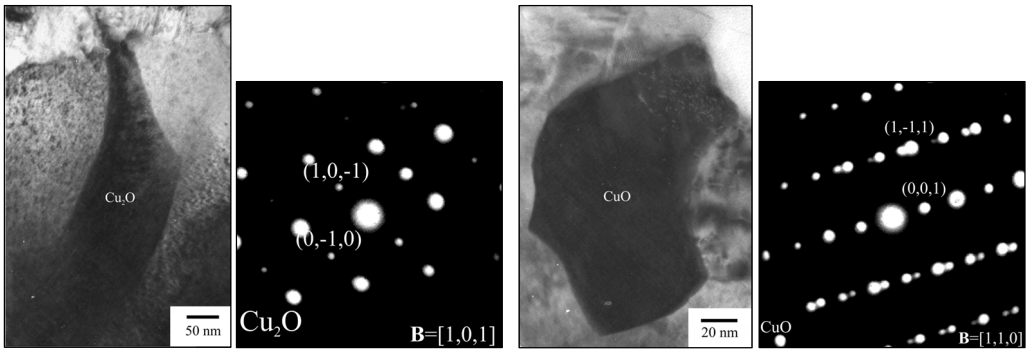

Figure 31. *Cu_2O and CuO grains, respectively, of Cu-DHP and their SAED patterns [Publication V].*

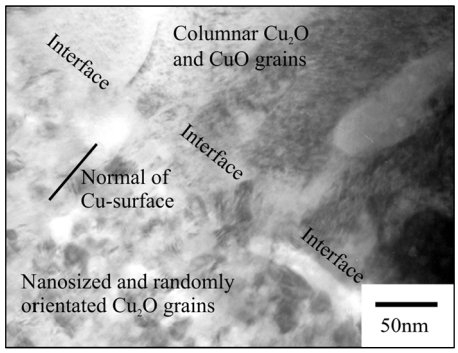

Figure 32. *Typical interface between Cu_2O layer and mixed oxide grains (Cu_2O and CuO) containing layer in alloyed copper [Publication V].*

The as-received, electrolytically polished, and oxidized surfaces of OFE-OK and Cu-DHP were studied with RAIRS. The spectra of OFE-OK (as-received, electrolytically polished, and oxidized in air at 200°C for 25 minutes) are presented in Fig. 33 [Publication VI]. As-received and electrolytically polished OFE-OK had a main peak at 650 cm^{-1} and a weak peak at 470 cm^{-1} indicating a mixed oxide structure Cu_2O and CuO [96], respectively, agreeing well with literature information about native oxide layer consisting of Cu_2O and CuO [73,74]. After the oxidation treatment at 200°C, OFE-OK had a very strong Cu_2O peak at 650 cm^{-1} which agrees well with TEM results [Publication V]. According to the intensities of the Cu_2O peaks, native copper oxide layers on the as-received and polished surface were much thinner than the oxide layer on the oxidized copper surface [Publication VI]. Also this finding agrees well with the literature indicating that the thickness of the native oxide layer is few nanometers [74]. TEM studies showed that the thickness of the oxide layer after 25 minutes oxidation at 200°C is ~40 nm [Publication V and VI]. The spectra of Cu-DHP copper were similar to those for OFE-OK [Publication VI]. Assignment of the RAIRS peaks and their locations are presented in Table 7.

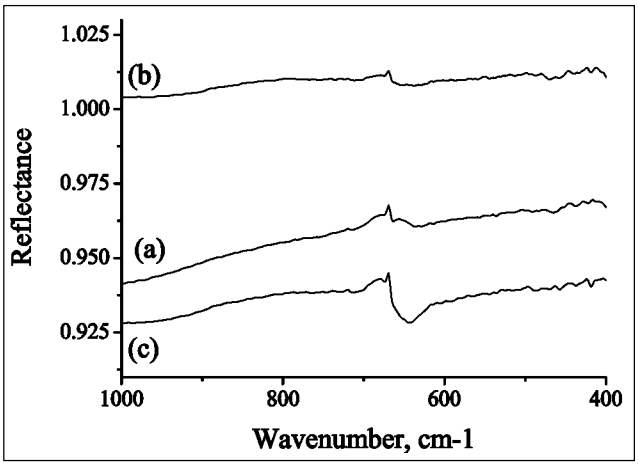

Figure 33. *RAIRS spectra of OFE-OK, wavenumber range from 1000 to 400 cm^{-1}, (a) as-received surface, (b) electrolytically polished surface, and (c) oxidized (in air at 200°C for 25 minutes) surface [Publication VI].*

The spectra of OFE-OK and Cu-DHP after oxidation treatment at 350°C for 25 minutes are presented in Fig. 34. Both copper grades had three peaks; OFE-OK had peaks at 655 and 590 cm^{-1} and a shoulder at 480 cm^{-1} and Cu-DHP had peaks at 650 and 610 cm^{-1} and a shoulder at 480 cm^{-1} [97]. The peak near 650 cm^{-1} indicates Cu_2O and the peaks at 590 / 610 cm^{-1} and 480 cm^{-1} indicate CuO [96]. Based on those peaks and assignments, mixed oxides, Cu_2O and CuO, formed during oxidation treatments at 350°C for 25 minutes. The intensity ratio CuO/Cu_2O was much higher for OFE-OK than for Cu-DHP indicating that OFE-OK had more CuO than Cu-DHP [97]. This agrees well with TEM results which showed that CuO layer formed on the Cu_2O layer in the case of OFE-OK and Cu_2O and CuO mixed layer in the case of Cu-DHP [Publication V]. Assignment of the RAIRS peaks and their locations and occurrence are presented in Table 7.

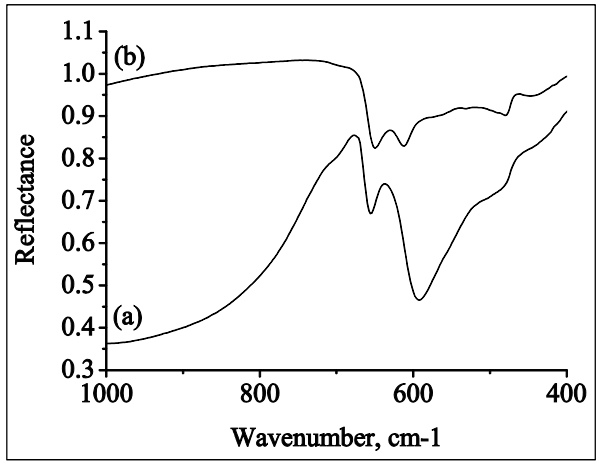

Figure 34. *RAIRS spectra, wavenumber range from 1000 to 400 cm^{-1} of (a) OFE-OK copper and (b) Cu-DHP after oxidation treatment in air at 350°C for 25 minutes [97].*

Table 7. *Assignment of RAIRS peaks, their locations, and occurrence in different samples [97].*

Location [cm^{-1}]	Assignment	Occurrence
650, 655	Cu_2O	All studied samples
590, 610	CuO	At 350°C oxidized OFE and DHP
470, 480	CuO	Polished OFE and DHP, at 350°C oxidized OFE and DHP

As a summary, schematic drawings of the oxide structures in the unalloyed (OF-OK) copper and alloyed (CuAg / Cu-DHP) copper after 100 minutes oxidation at 200 °C and after 25 or 100 minutes oxidation at 350 °C are presented in Fig. 35 [Publication V].

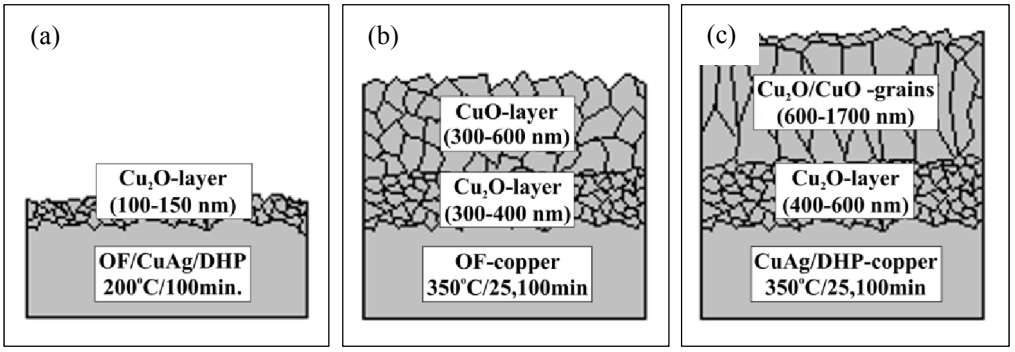

Figure 35. *Schematic drawings of oxide structures, (a) after 100 minutes oxidation at 200°C, (b) after 25 or 100 minutes oxidation at 350°C in case of OF-OK, and (c) after 25 or 100 minutes oxidation at 350°C in case of alloyed coppers (CuAg / Cu-DHP) [Publication V].*

OFE-OK and Cu-DHP were chosen as metallic parts for further studies of the copper-plastic hybrids. Subsequently, the oxidation treatment in air at 200°C for 25 minutes was chosen as an active surface modification for copper surfaces prior to silane treatment to improve silane bonding to the copper surfaces. With 25 minutes exposure, a dense, smooth, nanocrystalline, ~40 nm thick Cu_2O layer was achieved.

5.2.2. Silane layer on copper

Copper grades OFE-OK and Cu-DHP were used as metallic parts in the copper-TPU hybrids. Surface conditions used were: (1) cleaned, as-received, (2) electrolytically polished, and (3) electrolytically polished and oxidized in air at 200°C for 25 minutes. According to the oxidation studies of the copper grades, oxidation treatment resulted in ~40 nm thick dense Cu_2O layer. With longer exposure or at higher temperature, the formed surface oxide layer was thick, rough, porous, and contained mixture of Cu_2O and CuO oxides [Publications IV and V]. According to the initial studies, this kind of surface was not a good substrate for silane as the formed silane layer was nonuniform because of the rough surface.

Silane layers on the as-received, electrolytically polished, and oxidized (in air at 200°C for 25 minutes) OFE-OK and Cu-DHP surfaces, were produced using silane solution concentrations of 0.25 and 0.5 vol%. The layers were characterized with AFM, FESEM, TEM, and RAIRS.

Topographies of the copper surfaces before and after silane treatments were studied with AFM. The images of the oxidized OFE-OK surface without silane and with silane layers grown from the solution concentrations of 0.25 and 0.5 vol% are presented in Figs. 36 (a)–(c), respectively. The oxidized surface with the silane layer grown from the solution concentration of 0.25 vol% was rough and the underlying oxide structure was still observed indicating that the silane layer is thin and uneven (Fig. 36 (b)). In the case of the solution concentration of 0.5 vol%, the oxidized copper surface was flat and the oxide was covered by silane (Fig. 36 (c)). On the as-received copper surfaces, silane existed mainly in the rolling lines and on the polished copper surfaces (without oxide treatment) the silane layer was also uneven (not shown) [Publication VI].

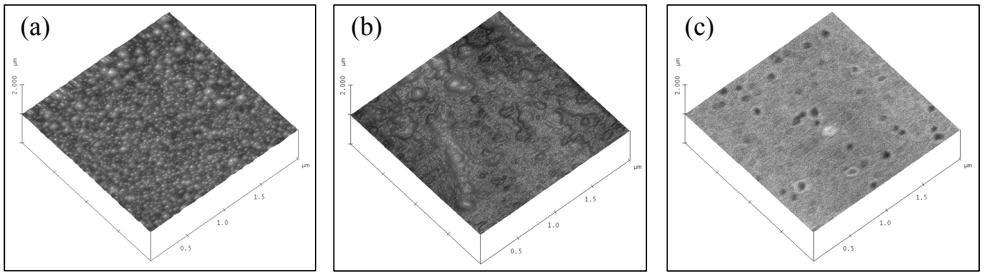

Figure 36. *AFM images of oxidized (in air at 200℃ for 25 minutes) OFE-OK surface (a) before silane treatment, (b) after silane treatment with solution concentration of 0.25 vol%, and (c) after silane treatment with solution concentration of 0.5 vol%. Scanned areas x = y = z = 2 µm [Publication VI].*

Silane layers were studied also with FESEM and TEM to get more detailed information about the uniformity and thickness of the layers. The FESEM images of the silane layers, grown from the solution concentration of 0.5 vol%, on the as-received and oxidized OFE-OK are presented in Figs. 37 (a) and (b), respectively. On the as-received OFE-OK surfaces, the silane layer thickness, grown from both solution concentrations, varied from a few nanometers to up to 100 nm. On the oxidized OFE-OK surface, silane layer was uniform and its thickness was ~25 nm and ~40 nm grown from the silane solution concentrations of 0.25 and 0.5 vol%, respectively. On the electrolytically polished copper surfaces, the silane layer was more uniform compared to the as-received surface but the layer thickness varied still from 20 to 100 nm and from 20 to 200 nm grown from the solution concentrations of 0.25 and 0.5 vol%, respectively (not shown). Situation was similar to Cu-DHP [Publication VI].

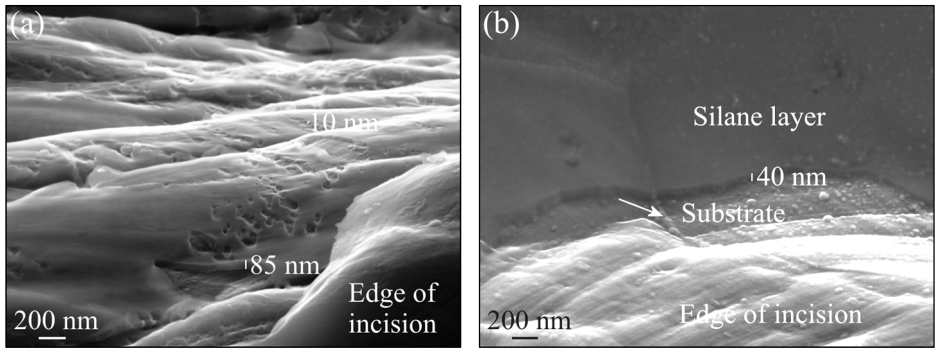

Figure 37. *FESEM images of silane layers (0.5 vol%) on (a) as-received OFE-OK and (b) oxidized OFE-OK, grain boundary area marked with arrow [Publication VI].*

The cross-sections of the silane layers were studied also with TEM. Images of the oxidized OFE-OK surface with silane layer, grown from the solution concentration of 0.25 vol%, are presented in Fig. 38. In the middle area of the copper grain, the silane layer thickness is about 25 nm and it is very uniform (Fig. 38 (a)) while, in the grain boundary area it is thin and irregular and hardly covers the oxide (Fig. 38 (b)). Situation was similar to Cu-DHP specimens [Publication VI].

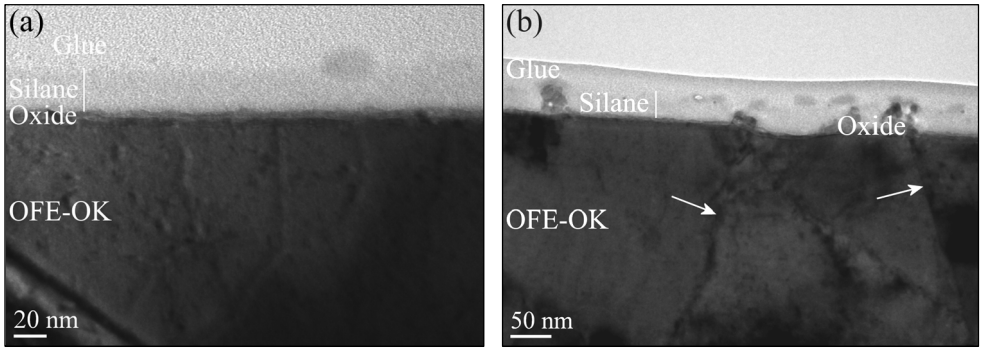

Figure 38. *TEM images of oxidized OFE-OK after silane treatment (0.25 vol%), (a) middle area of copper grain and (b) grain boundary area, arrows indicate grain boundaries. Notice different scale bars [Publication VI].*

TEM images of the oxidized copper surface with silane layer, grown from the solution concentration of 0.5 vol%, are presented in Fig. 39. In the middle area of the copper grain, the silane layer thickness is ~40 nm and it is uniform (Fig. 39 (a)). On the grain boundary area, the layer is thin but it covers the grain boundary and adjoining grain area (Fig. 39 (b)). According to TEM studies of the silane-treated coppers (Figs. 38 and 39), the underlying oxide layer is thinner than before silane treatment (Fig. 28) [Publication VI]. This is probably due to the solubility of copper oxide in the silane solution, as reported by Boerio *et al*. with γ-APS at pH 10.4 [29]. Probably, the relatively high pH value 9–10 of the silane solution used in this study caused dissolution of copper oxide into the solution. This was also noticed during the silane treatment; if many copper inserts were treated in the same solution, the color of the solution

changed from clear to lightly red, indicating existence of copper ions in the solution. Therefore, the silane solution was changed to fresh one frequently within silane treatments.

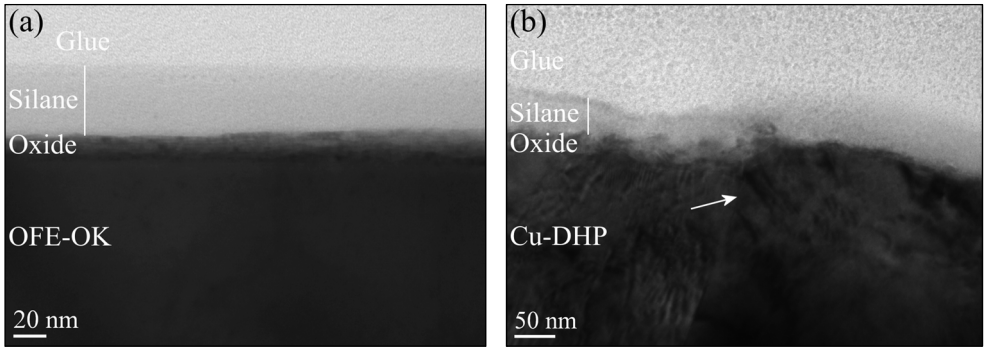

Figure 39. *TEM images of oxidized coppers after silane treatment (0.5 vol%), (a) middle area of copper grain (OFE-OK) and (b) grain boundary area (Cu-DHP), arrow shows grain boundary. Notice different scale bars [Publication VI].*

After silane treatments, the as-received and modified copper surfaces were studied with RAIRS. The spectra of the silane-treated Cu-DHP with the silane solution concentration of 0.5 vol% is presented in Fig. 40 and the assignments of the RAIRS peaks are given in Table 8. In all samples, the intense peaks at 1138 and 1046 cm^{-1} from the cross-linked SiOSi stretching vibrations were detected indicating that the silane layer polymerized during curing at 110°C for 10 minutes. However, in all Cu-DHP samples and in the polished OFE-OK samples treated with the solution concentration of 0.5 vol%, a weak peak or shoulder at 930 cm^{-1} was observed indicating small amount of unpolymerized silanols (located at 940 cm^{-1} according to [15]). In the polished samples, silane-treated with the solution concentration of 0.25 vol% (not shown), the peaks at 1138 and 1046 cm^{-1} were widened and the SiOSi band located at 1110 cm^{-1} indicating incomplete polymerization [98,99]. The band at 1590 cm^{-1} (in as-received and polished Cu-DHP, both silane concentrations) or 1585 cm^{-1} (in all other samples) was due to amine group deformation [29]. Boerio *et al.* studied γ-aminosilane films deposited at pH 10.4 on copper and they assigned a peak at 1580 cm^{-1} indicating deformation mode of amino groups coordinated to copper ions [29]. This peak was similarly assigned to hydrogen bonding of amino groups of γ-AEAPS on silica surface [99] and also to hydrogen bonding and complex formation with copper [98]. The wide hydrogen band at about 3300 cm^{-1} was observed in all oxidized samples. The amine peaks at 3420, 3520, and 3160 cm^{-1} were clearly observed in polished coppers, while for the as-received and oxidized samples those peaks were weak. It looks that the hydrogen band was not related to SiOH peak at 930 cm^{-1}, possibly this was related to absorbed water present in the thick layers [Publication VI].

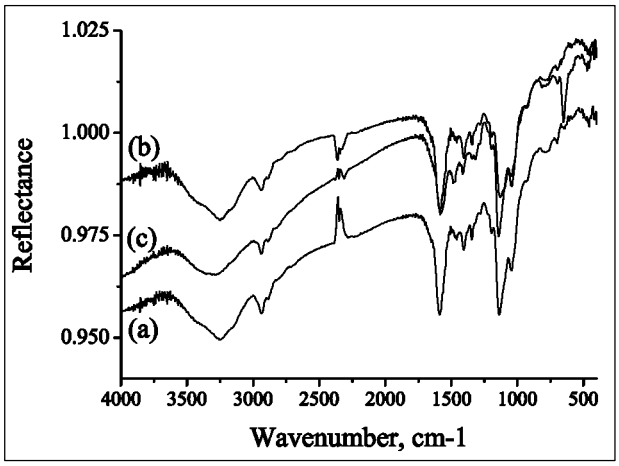

Figure 40. *RAIRS spectra of silanized (solution concentration 0.5 vol%) Cu-DHP surfaces, wavenumber range from 4000 to 500 cm^{-1}, (a) as-received surface, (b) polished surface, and (c) oxidized surface [Publication VI].*

Table 8. *Assignment of RAIRS peaks, their locations and occurrence [Publication VI].*

Location [cm^{-1}]	**Assignment**	**Occurrence**
3300	H_2O	oxidized OF and DHP
3420,3250, 3160	ν NH_2, NH	polished OF and DHP
2940	ν CH_2 as.	all samples
2885	ν CH_2 s.	all samples
1590	δ NH_2	all samples
1195	ρ $SiOCH_3$	all samples
1140	ν SiOSi as.	all samples
1045	ν SiOSi s.	all samples
930	ν SiOH	polished OF and all DHP
650	Cu_2O	oxidized OF and DHP

5.2.3. Hybrid structure

The peel strength values of the copper-TPU hybrids manufactured with different surface finishes of copper inserts are presented in Fig. 41. The copper insert surface has a significant effect on the formed silane layer and hence to the peel strength of the hybrid structure. The surface modifications, electrolytical polishing and oxidation, of the copper inserts improved the adhesion strength of the hybrids compared to the hybrids manufactured with as-received copper inserts. The rough surface due to rolling lines disturbed the silane layer formation in the as-received copper inserts resulting a nonuniform silane layer and hence poor adhesion strength of the hybrid. A smooth surface with Cu_2O layer produced by oxidation treatment was the good substrate for silane layer resulting in a thin, uniform, and cross-linked silane layer and hence well-bonded copper-TPU hybrids. Altough the electrolytically polished copper surface (without oxide treatment) was smooth, a native oxide layer was not good enough to form a uniform and well-bonded silane layer and therefore the peel strength values were significantly lower than with the oxidized copper insert [Publication VI].

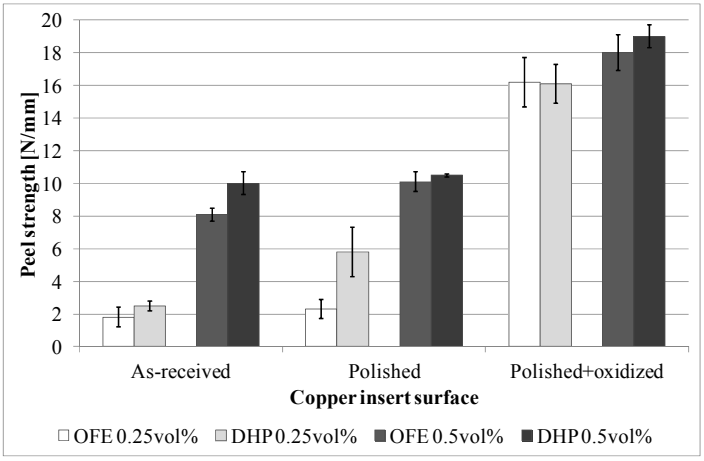

Figure 41. *Peel strengths of hybrids manufactured with various surface conditions of copper inserts, silane solution concentrations used were 0.25 vol% and 0.5 vol%, modified from [Publication VI].*

After the peel test, the failure surfaces were studied with an optical stereomicroscope (model MZ 7.5, Leica, Switzerland), AFM, FESEM, and RAIRS to get information about the failure types. The hybrids manufactured with oxidized copper inserts had about 40 % and 75 % cohesive failure in TPU depending on the silane solution concentrations of 0.25 and 0.5 vol%, respectively, determined with the aid of the optical stereomicroscope. With the as-received and polished inserts, no cohesive failure in TPU was detected. FESEM images of the failed surface (copper side) of hybrid manufactured with oxidized OFE-OK insert (silanized with 0.5 vol%) are presented in Fig 42. The cohesive failure in TPU (75%) is shown in Fig. 41 (a); the copper surface is totally covered by TPU. Also the RAIRS spectrum of that sample was similar to the reference TPU spectrum (not shown). FESEM images of the same sample from the remainder area (25 %) are presented in Figs. 42 (b) and (c); mainly adhesive failure between silane and TPU and failure inside the silane layer are detected. Even if, the oxide structure is weakly visible in Fig. 42 (c), silane remains on the oxide. Based on FESEM studies, the grain boundaries were not weak bonding areas, even if the formation of the silane layer had been

disturbed. This was concluded by the fact that the failure did not propagate along grain boundaries as shown in Fig. 42 (b). With the silane solution concentration of 0.25 vol%, less cohesive failure in TPU (40%) was achieved and the detected failure modes were adhesive failure between silane and TPU, failure in the silane layer, and adhesive failure between oxide and silane (not shown). Situation was similar in the hybrid manufactured with polished and oxidized Cu-DHP insert. [Publication VI].

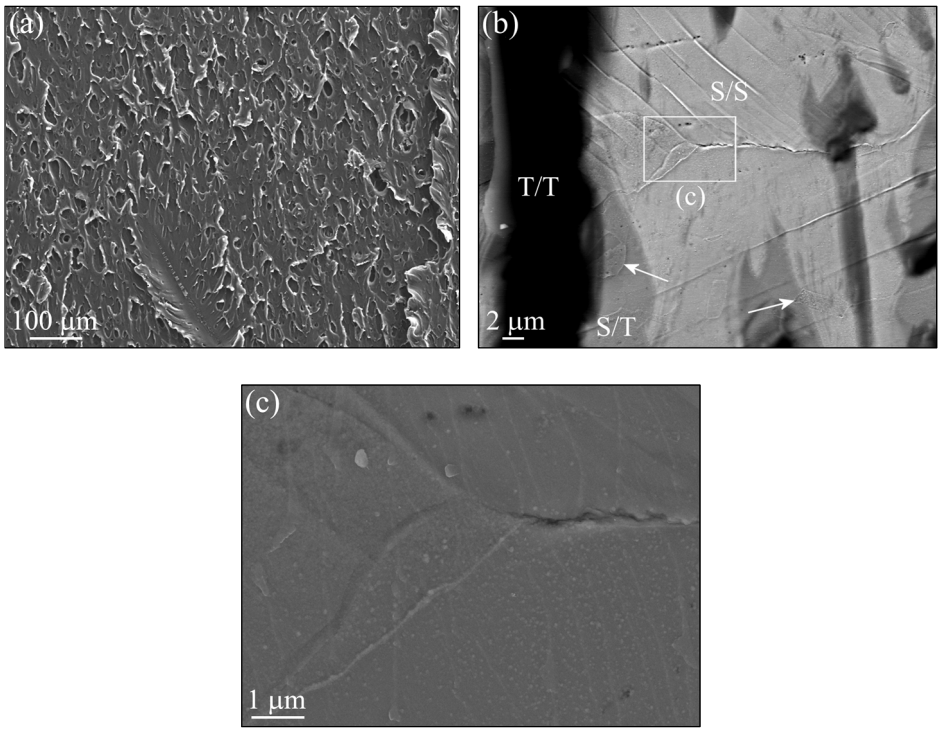

Figure 42. *FESEM images of failure surface (copper side) of copper-TPU hybrid manufactured with oxidized OFE-OK insert, silane solution concentration 0.5 vol%, (a) secondary electron (SE) image from area of cohesive failure in TPU (75%). (b) Angle-selective backscatter (AsB) image, some grain boundaries marked with arrows and (c) SE image from remainder failure area (25%). Failure types T/T is cohesive failure in TPU, S/T is adhesive failure between silane and TPU, S/S is failure in silane layer [Publication VI].*

In the failure surfaces of the hybrids manufactured with as-received OFE-OK and Cu-DHP (silane solution concentrations 0.25 and 0.5 vol%), no silane was detected with FESEM or AFM due to the too rough copper surface but with RAIRS, a weak peak related to silane was observed on the copper side, indicating failure in the silane layer or adhesive failure between silane and TPU. According to FESEM, AFM, and RAIRS studies, the hybrids manufactured with polished (without oxidation treatment) copper inserts failed in the silane layer (silane solution concentrations 0.25 and 0.5 vol%) and also adhesive failure between silane and TPU with 0.5 vol% silanized inserts was observed with AFM and FESEM [Publication VI]. Probably, mixed (Cu_2O and CuO) native oxide layers on the as-received and polished (without oxidation treatment) copper surfaces were too thin and typically contaminated by carbon [73] and therefore formation of a uniform and well-bonded silane layer was not possible. Oxidized copper surfaces were covered with a uniform, ~40 nm thick Cu_2O layer. Controlled oxide layer

slightly dissolved in silane solution so a thin, native oxide layer probably totally dissolved into the solution. This may to some extent disturb the silane layer formation [Publication VI].

6. CONCLUDING REMARKS

Injection-molded metal-plastic hybrids are innovative products combining dissimilar materials and their properties in the same component. Hybrids can offer benefits which are not achieved with individual material alone e.g.: savings in weight, part reduction, better dimensional stability, and manufacturing multi-functional components in a few processing steps. In this study, stainless steel-TPU and copper-TPU hybrids were prepared with injection molding. Chemical bonding between metals and plastic was produced with aminofunctional silane. Prior to silane treatment, surface modifications, i.e. electrolytical polishing and oxidation treatments, were carried out for stainless steel and coppers to improve silane bonding and hence metal-plastic adhesion. The effects of the modifications of the metal surfaces on the formation of the silane layers and the properties of the metal-plastic hybrids were studied. The hybrid structures were characterized within every manufacturing step with various research methods.

Silane bonding to the as-received metal surfaces was poor resulting in nonuniform silane layers. Oxidation treatments for stainless steel and copper surfaces were used to improve the bonding of the silane. To find out the optimal metal surface oxide structures, the oxidation behavior of stainless steels and coppers in various testing conditions were studied. Oxide structures of AISI 304 and AISI 316L were characterized after exposures in air at 350°C for 5–300 minutes. Oxidation behavior of both stainless steels was very similar. Oxidation started fast, already during the first 5 minutes exposure. The formed oxide layer was nanocrystalline M_2O_3-type. The layers were dense and their thickness after 100 minutes exposure was ~15 nm and after 300 minutes ~18 nm. According to the preliminary studies, the oxidation treatments in air at 350°C for 5 and 100 minutes were chosen as the surface modifications of the stainless steel inserts for stainless steel-TPU hybrid applications. Oxide structures of OF-OK/OFE-OK, Cu-DHP, and CuAg were studied after exposures in air at 200 and 350°C for 5–100 minutes. Under used testing conditions, the oxidation rate of alloyed coppers, Cu-DHP and CuAg, was faster than that of unalloyed OF-OK copper. With short exposure times, a nanocrystalline Cu_2O layer formed on all the studied coppers. At 350°C with 25 and 100 minutes exposure, the innermost layer was nano-sized Cu_2O. In the case of OF-OK copper, crystalline CuO layer grew on the Cu_2O layer. Columnar-shaped Cu_2O and CuO grains grew onto the Cu_2O layer on Cu-DHP and CuAg samples. According to the present studies, the oxidation treatment in air at 200°C for 25 minutes was chosen as the surface modification treatment of copper inserts for copper-TPU hybrid applications.

The surface finishes of the metal inserts have a significant effect on the formed silane layers. Silane layers on the as-received metal surfaces were nonuniform and existed mainly in the grain boundaries or in the rolling lines. XPS results indicated that the formation of a uniform silane layer on the as-received stainless steel surface was hindered by carbonous impurities on the surface, whereas oxidation treatment produced a clean Fe_2O_3-type surface oxide with improved bonding properties resulted in a uniform silane layer. In addition, the formed silane layer surface on the as-received stainless steel had less N (amino) species to react with TPU compared to the silane layer on the oxidized stainless steel surface. A thin and uniform silane layer with high cross-linking degree formed on the copper surface with a controlled Cu_2O layer, while the silane layers were uneven on the as-received and electrolytically polished copper surfaces. This means that a controlled oxide layer is needed to achieve a uniform and well-bonded silane layer.

Injection molding can be used to manufacture well-bonded metal-plastic hybrid structures. The metal surface, prior to silane treatment, affects significantly the formation of the silane layer and hence the peel strength and the failure types of the related injection-molded hybrids. The

hybrids manufactured with the as-received or electrolytically polished metal inserts failed mainly inside the silane layer with poor peel strength values. While, the hybrids manufactured with oxidized stainless steel or copper inserts failed mainly cohesively in TPU with high peel strength values. In a consequence, a modified metal surface with a controlled oxide layer and overlying a uniform, thin, and cross-linked silane layer is needed to achieve well-bonded metal-plastic hybrids. AFM, SEM, and TEM are good methods for quantitative and qualitative characterization of metal-plastic hybrids within different manufacturing steps. In order to prove that the developed surface treatments are relevant also in real applications, further studies on long-term stability must be carried out. In addition, the effect of the oxide and silane layer on the electrical conductivity, especially in the case of the OFE-OK-TPU hybrids, should be tested.

REFERENCES:

[1] http://techcenter.lanxess.com (31.1.2011).

[2] O. Zoellner and J. Evans, Plastic-metal hybrid a new development in the injection molding technology, ANTEC 2002 Plastics: Annual Technical Conference Proceedings, available at: www.knovel.com (29.4.2011).

[3] M. Grujicic, V. Sellappan, M. Omar, N. Seyer, A. Obieglo, M. Erdmann and J. Holzleitner, An overview of the polymer-to-metal direct-adhesion hybrid technologies for load-bearing automotive components, *Journal of Materials Processing Technology* 197 (2008) 363-373.

[4] G. Zhao and G. Ehrenstein, Investigation of a thin-walled thermoplastic metal hybrid, ANTEC 1999 Plastics: Annual Technical Conference Proceedings, available at: www.knovel.com (29.4.2011).

[5] C. Korson and D. Stratton, An integrated automotive roof module concept: plastic-metal hybrid and polyurethane composite technology, available at: www.bayermaterialsciencenafta.com (1.2.2011).

[6] G. Pritchard, Coupling agents, in: G. Pritchard (Ed.) Plastics Additives – An A-Z reference, Chapman & Hall, London, 1998, pp. 189-196.

[7] E. Plueddemann, Silane coupling agents, Plenum Press, New York, 1982.

[8] E. Petrie, Primers and adhesion promoters, in: Handbook of adhesives and sealants (second edition), McGraw-Hill, New York, 2007, pp. 277-305.

[9] D. Susac, X. Sun and K. Mitchell, Adsorption of BTSE and γ-APS organosilanes on different microstructural regions of 2024-T3 aluminum alloy, *Applied Surface Science* 207 (2003) 40-50.

[10] J. Kim, P. Wong, K. Wong, R. Sodhi, K. Mitchell, Adsorption of BTSE and γ-GPS on different microstructural regions of 7075-T6 aluminum alloy, *Applied Surface Science* 253 (2007) 3133-3143.

[11] F. Deflorian, S. Rossi and L. Fedrizzi, Silane pre-treatments on copper and aluminium, *Electrochimica Acta* 51 (2006) 6097-6103.

[12] F. Deflorian, S. Rossi, L. Fedrizzi and M. Fedel, Integrated electrochemical approach for the investigation of silane pre-treatments for painting copper, *Progress in Organic Coatings* 63 (2008) 338-344.

[13] R. Weterhold, E. Pisanova and H. Alarifi, Spray deposition methods for improving interfacial strength of copper-epoxy systems, *Journal of Adhesion Science and Technology* 24 (2010) 1221-1238.

[14] E. Petrie, Surfaces and surface preparation, in: Handbook of adhesives and sealants (second edition), McGraw-Hill, New York, 2007, pp. 227-275.

[15] F. Boerio, P. Shah, Adhesion of injection molded PVC to steel substrates, *Journal of Adhesion* 81 (2005) 645-675.

[16] http://www.insertech.net/10_insertmld.html (17.3.2011).

[17] www.taiseiplas.com (2.2.2011).

[18] M. Grujicic, V. Sellappan, G. Arakere, N. Seyer and M. Erdmann, Computational feasibility analysis of direct-adhesion polymer-to-metal hybrid technology for load-bearing body-in-white structural components, *Journal of Materials Processing Technology* 195 (2008) 282-298.

[19] http://www.insertech.net (18.3.2011).

[20] A. Al-Sheyaab, I. Kuehnert and E. Schmachtenberg, Insert coating as a pre-processing approach for improvement of adhesive bonding in plastic-metal hybrid structures, ANTEC 2007 Plastics: Annual Technical Conference Proceedings, available at: www.knovel.com (29.4.2011).

[21] T. Van Schaftinghen, C. Le Pen, H. Terryn and F. Hörzenberger, Investigation of the barrier properties of silanes on cold rolled steel, *Electrochimica Acta* 49 (2004) 2997-3004.

[22] W. van Ooij, D. Zhu, M. Stacy, A. Seth, T. Mugada, J. Gandhi and P. Puomi, Corrosion protection properties of organofunctional silanes – an overview, *Tsinghua Science and Technology* 10 (2005) 639-664.

[23] K. Weissenbach and H. Mack, Silane coupling agents, In: M. Xanthos (Ed.), Functional fillers for plastics, Wiley-VCH Verlag GmbH & Co., Weinhaim, 2005, pp. 59-83.

[24] V. Palanivel, D. Zhu and W. van Ooij, Nanoparticle-filled silane films as chromate replacements for aluminum alloys, *Progress in Organic Coatings* 47 (2003) 384-392.

[25] C. Bertelsen and F. Boerio, Linking mechanical properties of silanes to their chemical structure: an analytical study of γ-GPS solutions and films, *Progress in Organic Coatings* 41 (2001) 239-246.

[26] M.-L. Abel, R. Allington, R. Digby, N. Porritt, S. Shaw and J. Watts, Understanding the relationship between silane application conditions, bond durability and locus of failure, *International Journal of Adhesion & Adhesives* 26 (2006) 2-15.

[27] S. Torry, A. Campbell, A. Cunliffe and D. Tod, Kinetic analysis of organosilane hydrolysis and condensation, *International Journal of Adhesion & Adhesives* 26 (2006) 40-49.

[28] Y. Xie, C. Hill, Z. Xiao, H. Militz and C. Mai, Silane coupling agents used for natural fiber/polymer composites: A review, *Composites: Part A* 41 (2010) 806-819.

[29] F. Boerio, J. Williams and J. Burkstrand, The structure of films formed by γ-aminopropyltriethoxysilane adsorbed onto copper, *Journal of Colloid and Interface Science* 91 (1983) 485- 495.

[30] P. Jussila, H. Ali-Löytty, K. Lahtonen, M. Hirsimäki and M. Valden, Effect of surface hydroxyl concentration on the bonding and morphology of aminopropylsilane thin films on austenitic stainless steel, *Surface and Interface Analysis* 42 (2010) 157-164.

[31] P. Heiney, K. Grüneberg, J. Fang, C. Dulcey, R. Shashidhar, Structure and growth of chromophore-functionalized (3-aminopropyl)triethoxysilane self-assembled on silicon, *Langmuir* 16 (2000) 2651-2657.

[32] V. Subramanian and W. Van Ooij, Silane based metal pretreatments as alternatives to chromating, *Surface Engineering* 15 (1999) 168-172.

[33] S. Davis and J. Watts, Organization of methoxysilane molecules on iron, *International Journal of Adhesion and Adhesives* 16 (1996) 5-15.

[34] A. Franquet, J. De Laet, T. Schram, H. Terryn, V. Subramanian, W. Van Ooij and J. Vereecken, Determination of the thickness of thin silane films on aluminium surfaces by means of spectroscopic ellipsometry, *Thin Solid Films* 384 (2001) 37-45.

[35] Silane coupling agents: connecting across boundaries, Gelest technical library, available at: www.gelest.com (2.2.2011).

[36] M. Hoikkanen, M. Honkanen, M. Vippola, T. Lepistö and J. Vuorinen, Effect of silane treatment parameters on the silane layer formation and bonding to thermoplastic urethane, *Progress in Organic Coatings*, 2011, DOI 10.1016/j.porgcoat.2011.08.002.

[37] C. Le Pen, B. Vuillemin, S. Van Gils, H. Terryn and R. Oltra, In-situ characterization of organosilane film formation on aluminium alloys by electrochemical quartz crystal microbalance and in-situ ellipsometry, *Thin Solid Films* 483 (2005) 66-73.

[38] G. Li, X. Wang, A. Li, W. Wang and L. Zheng, Fabrication and adhesive properties of thin organosilane films coated on low carbon steel substrates, *Surface & Coating Technology* 201 (2007) 9571-9578.
[39] W. Yuan and W. van Ooij, Characterization of organofunctional silane films on zinc substrates, *Journal of Colloid Interface Science* 185 (1997) 197-209.
[40] J. Chovelon, L. Aarch, M. Charbonnier and M. Romand, Silanization of stainless steel surfaces: influence of application parameters, *Journal of Adhesion* 50 (1995) 43-58.
[41] I. De Graeve, E. Tourwé, M. Biesemand, R. Willem and H. Terryn, Silane solution stability and film morphology of water-based bis-1,2-(triethoxysilyl)ethane for thin-film deposition on aluminium, *Progress in Organic Coatings* 63 (2008) 38-42.
[42] D. Zhu, W. van Ooij, Corrosion protection of metals by water-based silane mixtures of bis-[trimethoxysilylpropyl]amine and vinyltriacetoxysilane, *Progress in Organic Coatings* 49 (2004) 42-53.
[43] S. Ebnesajjad, Surface treatment of materials for adhesion bonding, William Andrew Publishing, New York, 2006.
[44] K. Lawless, The oxidation of metals, *Reports on Progress in Physics* 37 (1974) 231-316.
[45] N. Cabrera and N. Mott, Theory of the oxidation of metals, *Reports on Progress in Physics* 12 (1948) 163-184.
[46] J. Yang, B. Kolasa, J. Gibson and M. Yeadon, Self-limiting oxidation of copper, *Applied Physics Letters* 73 (1998) 2841-2843.
[47] F. Fehlner and M. Graham, Thin oxide film formation on metals, in: P. Marcus (ed.), Corrosion mechanisms in theory and practice, Marcel Dekker Inc., New York, 2002, pp. 171-187.
[48] P. Jussila, Advances in nanoscale functionalization of stainless steel surfaces, Ph.D Thesis, Tampere University of Technology, Tampere, 2009.
[49] www.outokumpu.com (18.2.2011).
[50] S. Washko and G. Aggen, Wrought stainless steels, properties and selection: irons, steels, and high-performance alloys, in: ASM handbooks online Vol 1, ASM International, 1990, pp. 841-907.
[51] S. Kundu and H. Bhadeshia, Transformation texture in deformed stainless steel, *Scripta Materialia* 55 (2006) 779-781.
[52] J. Grubb, T. DeBold and J. Fritz, Corrosion of wrought stainless steels, corrosion: materials, in: ASM handbooks online Vol 13B, ASM International, 2005, pp. 54-77.
[53] B. Leffler, Stainless – stainless steels and their properties, available at: www.outokumpu.com/files/Group/HR/Documents/STAINLESS20.pdf (17.2.2011).
[54] C. Olsson and D. Landolt, Passive films on stainless steels – chemistry, structure and growth, *Electrochimica Acta* 48 (2003) 1093-1104.
[55] A. Vesel, M. Mozetic, A. Zalar, Oxidation of AISI 304L stainless steel surface with atomic oxygen, *Applied Surface Science* 200 (2002) 94-103.
[56] J. Tang, M. Halvarsson, H. Asteman and J.-E. Svensson, The microstructure of the base oxide on 304L steel, *Micron* 32 (2001) 799-805.
[57] W. Zielinski and K. Kurzydlowski, TEM studies of the oxide scales formed on type 316 stainless steel during annealing at 600°C in a vacuum and air, *Scripta Materialia* 43 (2000) 33-37.
[58] A. Johnson, D. Parsons, J. Mnzerova, D. Perry, D. Koury, B. Hosterman, J. Farley, Spectroscopic and microscopic investigation of the corrosion of 316/316L stainless steel by lead-bismuth eutectic (LBE) at elevated temperatures: importance of surface preparation, *Journal of Nuclear Materials* 328 (2004) 88-96.
[59] A. Greef, C. Louw, H. Swart, The oxidation of industrial FeCrMo steel, *Corrosion Science* 42 (2000) 1725-1740.

[60] S. Shieu, M. Deng and S. Lin, Microstructure and corrosion resistance of a type 316L stainless steel, *Corrosion Science* 40 (1998) 1267-1279.
[61] J. Lince, S Didziulis, D. Shuh, T. Durbin and J. Yarmoff, Interaction of O_2 with the $Fe_{0.84}Cr_{0.16}$ (001) surface studied by photoelectron spectroscopy, *Surface Science* 277 (1992) 43-63.
[62] K. Nomura and Y. Ujihira, Analysis of oxide layers on stainless steel (304 and 316) by conversion electron Mössbauer spectrometry, *Journal of Materials Science* 25 (1990) 1745-1750.
[63] S. Birosca and R. L. Higginson, Phase identification of oxide scale on low carbon steel, *Materials at High Temperatures* 22 (2005) 179-184.
[64] D. Tyler and W Black, Introduction to copper and copper alloys, properties and selection: nonferrous alloys and special-purpose materials, in: ASM handbooks online Vol 2, ASM International, 1990, pp. 216-240.
[65] www.luvata.com (16.2.2011).
[66] www.icsg.org (16.2.2011).
[67] B. Straumanis and L. Yu, Lattice parameters, densities, expansion coefficients and perfection of structure of Cu and of Cu-In α phase, *Acta Crystallographica* 25 (1969) 676-682.
[68] G. Zhou, TEM investigation of interfaces during cuprous island growth, *Acta Materialia* 57 (2009) 4432-4439.
[69] M. Lampimäki, K. Lahtonen, M. Hirsimäki and M. Valden, Nanoscale oxidation of Cu(100): Oxide morphology and surface reactivity, *The Journal of Chemical Physics* 126 (2007) 034703-1–034703-7.
[70] S. Lahiri, N. Waalib Singh, K. Heng, L. Ang and L. Goh, Kinetics of oxidation of copper alloy leadframes, *Microelectronics Journal* 29 (1998) 335-341.
[71] J. Yang, M. Yeadon, B. Kolasa and J. Gibson, Oxygen surface diffusion in three-dimensional Cu_2O growth on Cu(100) thin films, *Applied Physics Letters* 70 (1997) 3522-3524.
[72] J. Yang, M. Yeadon, B. Kolasa and J. Gibson, The homogeneous nucleation mechanism of Cu_2O on Cu(001), *Scripta Materialia* 38 (1998) 1237-1242.
[73] S. Suzuki, Y. Ishikawa, M. Isshiki and Y. Waseda, Native oxide layers formed on the surface of ultra high-purity iron and copper investigated by angle resolved XPS, *Materials Transactions, JIM*, 38 (1997) 1004-1009.
[74] J.-W. Lim, J. Iijima, Y. Zhu, J. Ho Yoo, G.-S. Choi, K. Mimura and M. Isshiki, Nanoscale investigation of long-term native oxidation of Cu films, *Thin Solid Films* 516 (2008) 4040-4046.
[75] S. Ghosh, D. Avasthi, P. Shah, V. Ganesan, A. Gupta, D. Sarangi, R. Bhattacharya, W. Assman, Deposition of thin films of different oxides of copper by RF reactive sputtering and their characterization, *Vacuum* 57 (2000) 377-385.
[76] K. Lahtonen, Oxygen adsorption-induced nanostructures on copper and silver-copper alloy surfaces investigated by scanning tunneling microscopy and electron spectroscopy, PhD thesis, Tampere University of Technology, Tampere, 2008.
[77] J.-H. Park and K. Natesan, Oxidation of copper and electronic transport in copper oxides, *Oxidation of Metals* 39 (1993) 411-435.
[78] Y. Zhu, K. Mimura and M. Isshiki, Influence of small amounts of impurities on copper oxidation at 600-1050°C, *Oxidation of Metals* 59 (2003) 575-590.
[79] Y. Zhu, K. Mimura, M. Isshiki, A study of the initial oxidation of copper in 0.1 MPa oxygen and the effect of purity by metallographic methods, *Corrosion Science* 46 (2004) 2445-2454.

[80] M. Lampimäki, K. Lahtonen, M. Hirsimäki and M. Valden, Oxidation-induced nanostructures on Cu{100}, Cu(Ag) and Ag/Cu{100} studied by photoelectron spectroscopy, *Surface and Interface Analysis* 39 (2007) 359-366.
[81] http://www.outokumpu.com/applications/upload/pubs_102110190.pdf (22.2.2011).
[82] http://www.outokumpu.com/43395.epibrw (22.2.2011).
[83] http://www.outokumpu.com/33393.epibrw (22.2.2011).
[84] http://www.outokumpu.com/About-stainless/Steel-Properties/Surfaces/5876/Cold-Rolled/ (14.9.2011).
[85] A guide to silane solutions, available at: www.dowcorning.com (4.3.2011).
[86] http://www.plasticsnews.com/headlines2.html?id=19994&q=estane (4.3.2011).
[87] M. Honkanen, M. Hoikkanen, M. Vippola, J. Vuorinen, T. Lepistö, Electron microscopy of silane layers in stainless steel-TPU hybrids, in: Proceedings of 61st Annual Meeting of the Scandinavian Society for Electron Microscopy, Stockholm, Sweden, June 8-10, 2010.
[88] M. Vippola, Microstructural Study of Aluminum Phosphate Sealed Plasma Sprayed Alumina and Chromia Coatings, PhD thesis, Tampere University of Technology, Tampere, 2002.
[89] N. Fairley, CasaXPS: Spectrum Processing Software for XPS, AES and SIMS (Version 2.3.13), Casa Software Ltd, Cheshire, 2006, available at: http://www.casaxps.com/.
[90] C.D. Wagner, A.V. Naumkin, A. Kraut-Vass, J.W. Allison, C.J. Powell and J.R. Rumble Jr., NIST XPS Database, Version 3.5 (Web Version), National Institute of Standards and Technology, 2007, available at: http://srdata.nist.gov/xps/.
[91] JCPDS No. 38-1479, International Center for Diffraction Data (ICDD), Powder Diffraction File Database 1999.
[92] L. Finger and R. Hazen, Crystal structure and isothermal compression of Fe_2O_3, Cr_2O_3, V_2O_3 to 50 kbars, *Journal of Applied Physics* 51 (1980) 5362-5367.
[93] JCPDS No. 33-664, International Center for Diffraction Data (ICDD), Powder Diffraction File Database 1999.
[94] H. Cabibil, V. Pham, J. Lozano, H. Celio, R.M. Winter, J.M. White, Self-organized fibrous nanostructures on poly[(aminopropyl)siloxane] films studied by atomic force microscopy, *Langmuir* 16 (2000) 10471-10481.
[95] JCPDS No. 5-667, International Center for Diffraction Data (ICDD), Powder Diffraction File Database 1999.
[96] B. Lefez, R. Souchet, K. Katrouni and M. Lenglet, Infrared reflection study of CuO in thin oxide films, *Thin Solid Films* 268 (1995) 45-48.
[97] M. Honkanen, M. Hoikkanen, M. Vippola, J. Vuorinen, and T. Lepistö, unpublished results.
[98] X. Gu, G. Xue and B. Jiang, Effect of deposition conditions for γ-aminopropyltriethoxy silane on adhesion between copper and epoxy resins, *Applied Surface Science* 115 (1997) 66-73.
[99] C.-H. Chiang and J. Koenig, Fourier transfrorm infrared spectroscopic study of the adsorption of multiple amino silane coupling agents on glass surfaces, *Journal of Colloid and Interface Science* 83 (1981) 361-370.